Review

Titanium Dioxide and Photocatalytic CO2 Reduction: A Detailed Review of the Current Status and Future Prospects

Dilshod Nematov *

Posted Date: 15 January 2025

doi: 10.20944/preprints202501.1197.v1

Keywords: catalytic reactions; photocatalysis; charge separation; titanium dioxide; brookite TiO2; photocatalytic CO2 reduction; water splitting; hydrogen production

Review

Titanium Dioxide and Photocatalytic CO2 Reduction: A Detailed Review of the Current Status and Future Prospects

Dilshod D. Nematov

Quantum Electronics Laboratory, S.U. Umarov Physical-Technical Institute of National Academy of Sciences of Tajikistan, Dushanbe, Tajikistan; dilnem@mail.ru

Abstract: A significant amount of carbon dioxide is released into the atmosphere as a result of the extensive usage of fossil fuels. The photocatalytic reduction and conversion of CO2 under visible light into alternative renewable solar fuels or other oxygenated products (methane, formaldehyde, methanol, and formic acid) are practical and efficient methods for reducing atmospheric carbon pollution. Functional materials containing titanium dioxide (TiO2) have attracted significant interest for the photocatalytic reduction of CO2. In this direction, many studies have been conducted in recent years, especially on solar energy harvesting and the charge separation, adsorption, activation, and reduction of CO2 on enhanced TiO2. Recent studies have shown that brookite TiO2 (BT) was the most active photocatalyst, followed by rutile and anatase. Therefore, this study aims to review in detail the recent advances in the development of selective and active catalysts for photocatalytic CO2 reduction using titanium dioxide with a brookite structure. Therefore, a review is provided to evaluate the most common methods for obtaining BT. Then, developed engineering strategies such as doping with metallic or non-metallic heteroatoms, addition of a co-catalyst, formation of heterojunctions, and other algorithms to improve the CO2 reduction mechanism are discussed. The influence of another phase and crystal facets on the photocatalytic CO2 reduction reaction are discussed in detail. The problems associated with BT-based photocatalysts, namely, their modest visible-light absorption, slow interfacial charge separation, and poor surface catalytic dynamics, are further discussed, along with possible solutions. To stimulate additional research in this field, the difficulties and potential advantages of photocatalytic CO2 conversion methods are discussed.

Keywords: catalytic reactions; photocatalysis; charge separation; titanium dioxide; brookite TiO2; photocatalytic CO2 reduction; water splitting; hydrogen production

1. INTRODUCTION

Technologies for converting solar energy into hydrogen emission reaction or CO2 reduction reaction (CO2RR) have attracted a lot of interest as potential solutions to the energy and environmental problems brought on by the extensive use of fossil fuels[1]. The use of fossil fuels has become a sword of Damocles, looming over human society because of environmental damage, energy scarcity, and the greenhouse effect [2–5]. It is crucial to discover new environmentally beneficial ways to convert CO2 into clean and sustainable energy. Hydrocarbon fuels (CH)4, CH3OH, CO, and other hydrocarbons can be produced from CO2 using semiconductor photocatalytic CO2, which replicates plant photosynthesis.

In addition, they can reduce the effects of energy crises and environmental degradation [5–11]. The following procedures are primarily involved in CO2 recovery on solar cells: (a) the catalyst absorbs photon energy to form photogenerated carriers and adsorbs the CO2 molecules on its surface; (b) photogenerated electrons and holes separate and diffuse onto the photocatalyst surface; and (c) once on the surface, the electrons and holes start oxidation and reduction reactions (Figure 1). Problems with charge mobility dynamics and the impact of thermodynamic variables characterize

 doi:10.20944/preprints202501.1197.v1

these three processes. First, the photon energy directly affects the excitation of semiconductor electrons in terms of thermodynamic considerations [12].

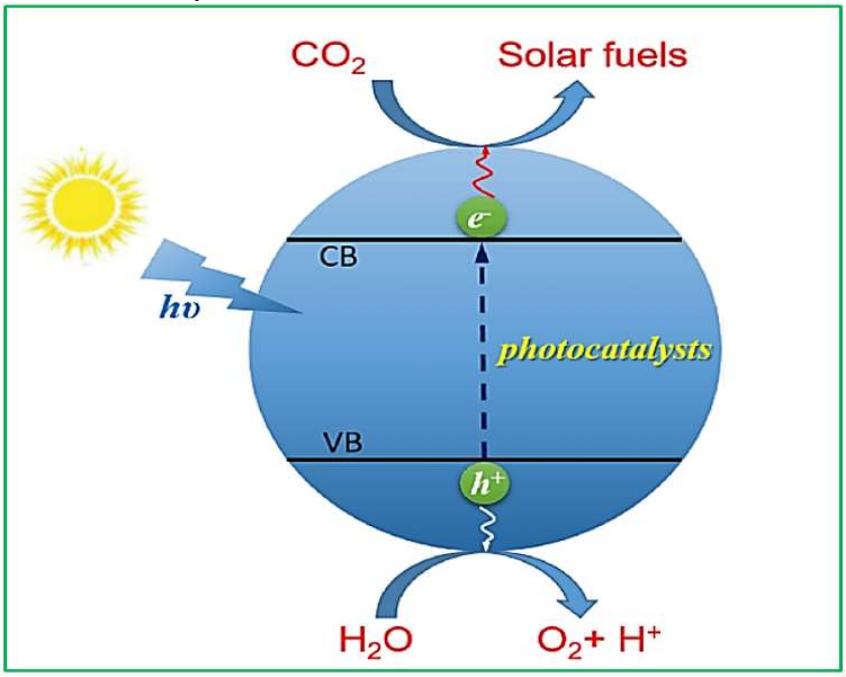

Figure 1. Simple CO2 Photocatalytic Reduction Scheme Using Semiconductor Photocatalysts.

While CO2 is a linear molecule that needs to absorb sufficient energy to break the C=O bond, semiconductors must have a sufficiently high reducing power to reduce CO2 to other substances, and their reducing power is primarily related to the position of the conduction band (CB) of the semiconductor [12]. In contrast, electrons can be excited by incident light from the valence band (VB) to the CB only if the photon energy is equal to or greater than the bandgap of the semiconductor. Consequently, semiconductors must be located further away from the reduction potential and closer to the negative CB. From a kinetic perspective, the separation or migration efficiency of photogenerated carriers determines the rate of CO2 photoreduction; light harvesting has a significant influence on this rate, and the selectivity of the reduction products is directly related to the desorption of reactants and intermediates. The three main crystalline phases of TiO2 found in nature are rutile, brookite, and anatase [13–18]. The TiO6 octahedrons (Figure 2) form the fundamental unit of all three crystal structures. The differences between the three crystal forms can be explained by the distortion and interconnected [13]. The tetragonal system includes anatase and rutile, whereas the rhombic system includes brookite [18–22].

 doi:10.20944/preprints202501.1197.v1

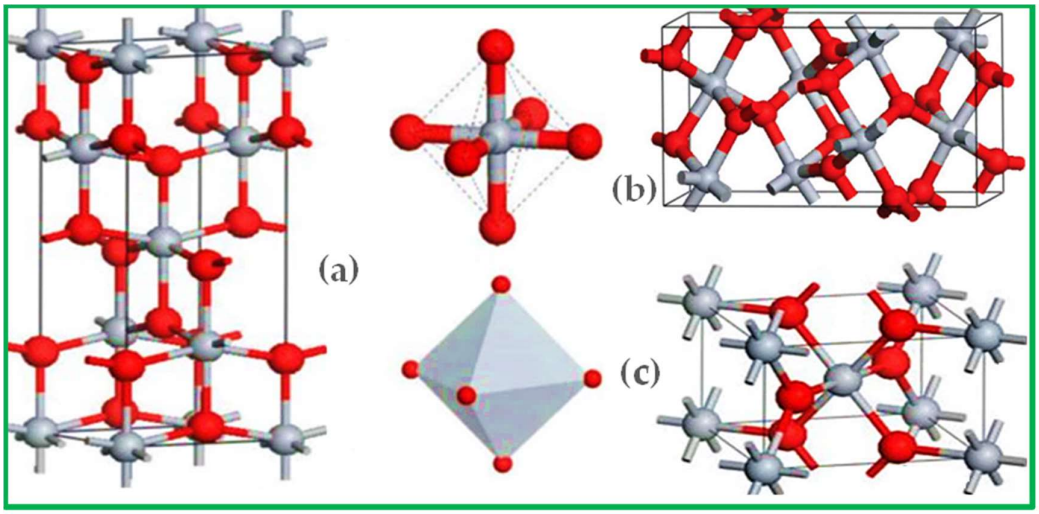

Figure 2. Crystal Structures of TiO2 (A) Anatase (Tetragonal), (B) Brookite (Orthorhombic), and (C) Rutile (Tetragonal) polymorphs.

Recent studies on the properties of TiO2 catalysts and their photocatalytic performance have shown that, despite its relatively low stability, brookite was found to be the most active photocatalyst, followed by rutile and anatase [18–22]. The high activity of brookite, confirming the importance of the crystal structure for photoreformation, is attributed to efficient charge-transfer kinetics, a slow decomposition rate, abundant formation of •OH radicals, and moderate electron trap depth, which can easily motivate researchers and stimulate further research in this area.

BT exhibited much lower crystal symmetry than anatase and rutile. The most stable crystalline phase is rutile, and the TiO2 octahedra undergo significant deformation [13–22]. Compared with rutile and anatase, the brookite phase is less common because it is more difficult to obtain in pure form. However, the unique configuration of octahedral TiO6 in the crystal structure of brookite leads to the formation of channels along the C-axis of the crystal. Because some small cations can bind to these channels, brookite may have applications in the field of catalysis [22]. In addition, owing to the unique octahedral chain connection, the O atoms are in the {1 0 0} crystal plane, and they can be used as catalytically active atoms [23]. The three crystalline TiO2 samples exhibited different electron band configurations because of these structural variations. Most studies to date show that the forbidden band widths (Eg) of brookite, rutile, and anatase are 3.2, 3.0, and 3.2eV, respectively [24–28]. Fattah-Alhosseini et al.investigated the effect of CuSO4 addition on the variation of current density, trisodium phosphate concentration, forbidden zone width, microstructure, and photocatalytic efficiency of visible-light-activated TiO2 coatings and showed that increasing the current density from 6 to 18A/dm2 increases the pore size in the coating. Phase analysis of the oxide coating showed that increasing the current density from 6 to 18A/min decreased the proportion of the rutile phase in the coating. Further introduction of 4g/L CuSO4 into phosphate- and hydroxide-based electrolytes resulted in Cu(OH)2 precipitation, which destabilized the electrolyte. To stabilize it, potassium hydroxide was removed, and the optimum concentration of trisodium phosphate salt was determined. Numerous studies have shown that brookite has the highest Fermi level and a negative CB position, making it suitable for photocatalytic CO2 reduction.

The three types of TiO2 listed above undoubtedly have the following disadvantages: low photon absorption, rapid recombination of photogenerated electrons and holes, and an inevitable reverse reaction. Therefore, much work has been done to address these problems and improve the photocatalytic reduction potential of CO2. In particular, studies have been conducted to obtain and modify anatase-phase TiO2 and its materials in terms of their macroporous structure [30], response

 doi:10.20944/preprints202501.1197.v1

to visible light [30], and crystal facet control [26–30]. However, to the best of our knowledge, no studies on the CO2 photoreduction of BT materials have been conducted. As early as the last century, brookite was found to exhibit greater photocatalytic activity than rutile and anatase [31]. The majority of research has focused on five areas: phase transition regulation, cocatalyst loading, heteroatom doping, crystal face regulation, and heterostructure creation. Brookite TiO2 can be regulated by the aforementioned modifications to maximize the charge separation/transfer, surface active centers, and solar energy harvesting for photocatalytic CO2 reduction.

In recent years, there has been an increase in research interest in the design of CO2-based BT photocatalysts; nevertheless, clarification of the impact of particular modification strategies on the photocatalytic performance is still required. This paper provides an overview of recent developments and efforts to develop BT photocatalysts for CO2 reduction, given the ongoing advances in the production and modification of this material. This study constitutes the first report on TiO2 synthesis strategies of TiO2 been reported. The modification of TiO2-based photocatalysts in the brookite phase for CO2 amplification was carefully evaluated. The possibility of reduction was also examined. The results also demonstrate how the triggered modification methods improve performance. Finally, we provide an overview of the results and discuss the opportunities and challenges associated with the use of BT photocatalysts for photocatalytic CO2 reduction. Because of its chemical stability, non-toxicity, and affordability, titanium dioxide has thus been the most extensively employed "promising" photocatalyst in heterogeneous photocatalysis [32,33]. In the past two decades, heterogeneous photocatalysis of titanium dioxide has spread very rapidly, undergoing various energy and environmental challenges such as direct solar splitting of H2O into H2 and decomposition of pollutants [33]. Although much progress has been made in heterogeneous TiO2 photocatalysis, much remains unknown, which poses an interesting challenge not only to engineers but also to basic research scientists. Generally, a typical TiO2 photocatalytic reaction contains many fundamental processes, including charge carrier formation, separation, relaxation, trapping, transport, recombination and transport, and bond breaking/forming, which need to be thoroughly investigated. Only when all these fundamental processes are clearly identified can a better understanding of TiO2 photocatalysis be achieved [32,33], which is vital for the development of new photocatalysts and the characterization of new photocatalytic processes.

Thus, a series of scientific articles have been devoted to the synthesis and application of brookite for the photocatalytic reduction of carbon dioxide, but, despite this, many aspects of this problem remain unclear. For example, there is still insufficient data to fully understand how photogenerated charge carriers contribute to bond formation and breaking in TiO2 photocatalysis, which is crucial for unraveling the nature of TiO2 photocatalysis. Fundamental studies using surface studies are needed to obtain a deeper understanding of these processes. In this review, we aim to provide a comprehensive overview of TiO2 photocatalysis to identify and clarify the direction of future research in this field.

2. EFFICIENT METHODS AND TECHNOLOGIES FOR THE PREPARATION OF BT

TiO2-based functional materials can be synthesized using various physicochemical methods [33]. The most common methods for the preparation of BT are hydrothermal method [34], sol-gel method [35–38], solvothermal method [39–42], thermal decomposition method [43,44], high temperature amine hydrolysis method [45], vapor deposition method [46,47] and other improved methods. The following paragraphs describe the process for obtaining titanium dioxide BT using specific techniques. The hydrothermal method for obtaining titanium dioxide with a brookite structure has received special attention for its use in photocatalytic reactions involving CO2 [48].

 doi:10.20944/preprints202501.1197.v1

2.1. Hydrothermal Synthesis of BT

The hydrothermal method involves encapsulating a mixed system with deionized water as the solvent and a source of titanium in an autoclave in an oven to produce a sample at a specific temperature and time. This approach allows for easy control of the shape and process of brookite production. TiO2 sources such as TiO2 nanoparticles [48], titanium hydroxide particles [49], TiCl4 [50], titanium foil [51], titanium butoxide [52], and similar materials are now widely used to create brookite TiO2. Studies on photocatalysts with unique morphologies and structures have been quite active. Thus far, the hydrothermal approach has been used to create BT with a variety of architectures, such as nanoparticles, nanites, and nanotubes [53–57].

Using a water-soluble titanium glycolate complex as a precursor, Tomita et al.in 2012 obtained amphiphilic BT nanoparticles via hydrothermal growth modified with sodium oleate. These nanoparticles can diffuse widely in cyclohexane and water, indicating their efficiency in the synthesis of amphiphilic nanoparticles. In agreement with previous findings, high Na concentrations were found to promote the formation of brookite TiO2 [59]. The amphiphilic brookite nanoparticles exhibited remarkable photocatalytic activity. The development of dye-sensitized solar cells was improved by combining TiCl4 with urea and deionized water [60]. Using a simple hydrothermal process and water-soluble titanium and amino acid complexes as morphological and structural agents, Xu J et al.fabricated TiO2 nanoparticles with tunable crystalline phases, sizes, and morphological structures. By treating the precursors with different amino acids, brookite can exhibit different morphologies. Using TiS2 as a precursor in a NaOH solution, Chen et al.created highly crystalline nanostructures of pure brookite and biphasic anatase/brookite TiO2 using a simple hydrothermal process. The phase composition can be adjusted by varying the solution concentration and reaction time. The effects of NaOH concentration and reaction time on the TiO2 crystals are shown in Figure 3A and 3B, respectively.

 doi:10.20944/preprints202501.1197.v1

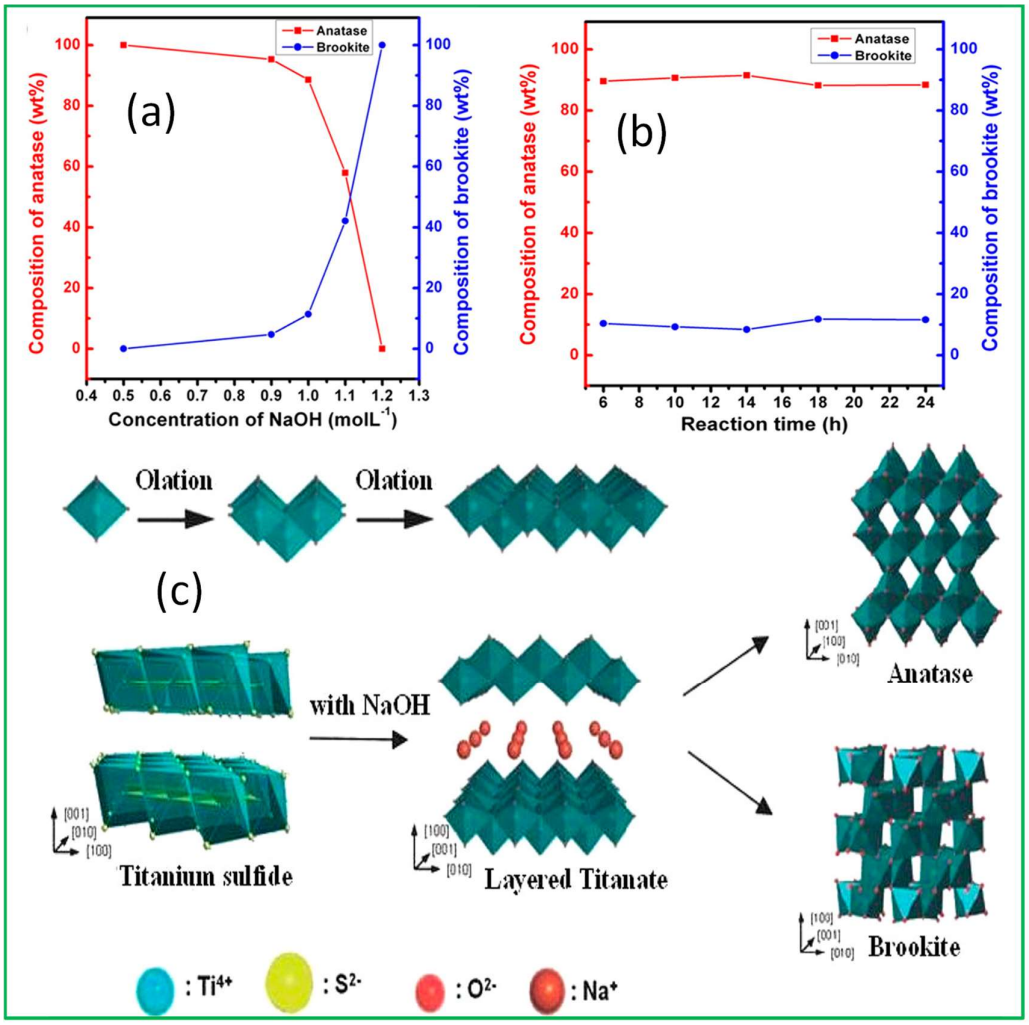

Figure 3. The Compositions of Anatase and Brookite in Mixed-phase TiO2 Synthesized. A: with various NaOH concentrations; B: Reaction Times under Hydrothermal Reaction; C: The Scheme of Formation of Anatase and Brookite. Reproduced from Ref.with Permission from American Chemical Society.

At the beginning of the reaction, TiS2 was hydrolyzed to form Ti4+ (Figure 3A). The Ti4+ and OH- in the solution interacted during the hydrothermal process (Figure 3B). Anatase TiO2 is formed at low OH concentrations because it leads to a low rate of hydrolysis of Ti4+. Conversely, high OH- concentration causes a high rate of Ti4+ hydrolysis, resulting in the formation of a mixed phase of TiO2 (brookite and anatase). The graphs show that the brookite content increased with increasing NaOH concentration, whereas the crystalline form of the product did not change significantly when the reaction time exceeding 6h. In addition, sodium titanate can be converted to brookite. Because Na+ can stabilize the layered structure, when Na+ is absent from the reaction system, the layered structure becomes unstable and is broken down by the hydrothermal process to form TiO2 anatase. When Na+ is present in excess, the layered structure is very stable and eventually forms titanate. At moderate Na+ concentrations, the layered structure is partially destroyed and part of it remains unstable, forming brookite (Figure 3C) [61].

Controlling the crystal shape and shape is crucial for the photocatalytic CO2 reduction. Rice-like BT was produced by Li et al.using high-temperature calcination and hydrothermal reactions. The shape of the BT is significantly influenced by a number of factors, including hydrothermal reaction time, titanium concentration, and calcination temperature. The crystal phase of BT is significantly

 doi:10.20944/preprints202501.1197.v1

altered when the calcination temperature is too high (>800°C). Kominami et al.produced microcrystalline TiO2 brookite with a high specific surface area by solvothermal treatment.

As the temperature increased to 700°C, the brookite became entirely rutile. The findings demonstrated that the presence of Na or K alkaline metal ions is critical for the nuclear growth of BT and embryo formation and inhibits the growth of the rutile or anatase phases. The produced samples have a uniform particle size and good purity, and the solvothermal process tends to control the size, shape distribution, and crystallization of TiO2 nanoparticles better than the hydrothermal method.

After combining titanium hydroxide with ammonium lactate, urea, and deionized water, Yang et al.hydrothermally produced one-dimensional BT nanorods. Its crystal planes are of two sizes: a larger {2 1 0} open crystal and a smaller {2 1 2} exponential crystal. The photocatalytic breakdown activity of acetaldehyde was also enhanced by increasing the side ratio following the inclusion of polyvinyl alcohol (PVA) or polyvinylpyrrolidone (PVP) as a side-ratio control agent.

This is because the oxidation-reduction reaction takes place on separate crystal facets, which increases the photocatalytic activity as a result of the equivalent surface areas {2 1 0} and {2 1 2} of the exposed crystalline facets of the reduction and oxidation sites. Since then, titanium hydroxide (BIS) and carbamide have been used as raw ingredients by other researchers to create BT nanostructures using a slightly modified version of this technique [65,66]. The chemicals used to adjust pH differed.

A new approach to low-alkalinity solution chemistry was developed by Lin et al.As shown in Figure 3A and 3B, TiCl4 evolved into a strong acid solution after the formation of the water-soluble complex [Ti(OH)2(O2)4]2+. The combination then forms the brookite precursor [Ti(C3H4O3)3]2 upon the addition of sodium lactate and urea, and hydrothermal processes result in the formation of brookite nanolists. In comparison with the other configurations, the nanosheets exhibit superior photocatalytic activity. The results demonstrated that the photocatalytic activity of BT was significantly influenced by its shape, suggesting a novel method for enhancing the activity of BT.

TiO2 nanoflowers were produced by Huang et al.using a one-step hydrothermal process involving tetrabutyltitanate, NaCl, and NH3-H2O. Nanorods of approximately 40nm were used to fabricate various floral shapes. It was discovered that, whereas NH+4+ could not stabilize the structure because of its quick conversion to NH3-H2O in solution and its inability to supply a positive charge to stabilize the negatively charged titanate layer, Na could stabilize the layered floral structure.

Notably, the photocatalytic performance of BT was greatly enhanced by its hierarchical structure and the presence of oxygen vacancies in the crystal. By employing TiOSO4 as the raw material and NaOH or HNO3 as a pH adjuster, Li et al.created BT nanoflowers using a hydrothermal process. The generation of BT nanoflowers depends on the pH and formation of alkali metals. Anatase and rutile are more likely to nucleate when exposed to alkali metal ions, whereas sodium ions can encourage the nucleation of brookite. Other types of amorphous brookite can also be produced by hydrothermal methods. Using TiCl4, H2O, and concentrated hydrochloric acid as raw materials, Bellardita et al.created a mixed phase of rutile and brookite using the hydrothermal method. Ash exposure was used to separate brookite and rutile and to produce pure brookite nanoparticles by repeatedly discarding the supernatant and adding water to return the solution volume to its original state. Scanning electron microscopy revealed that the structure was an amorphous, friable, and porous material. Owing to the disadvantages of this method, including the low crystallinity of the final product and high energy consumption in mass production, we believe that it is necessary to take appropriate precautions and investigate other methods of brookite synthesis.

 doi:10.20944/preprints202501.1197.v1

2.2. Sol-gel Method of BT Synthesis

Titanium precursor hydrolysis is the primary method used in the sol-gel production of TiO2. The precursors included titanium tetrachloride and titanium alkoxide. Hydrolysis of the titanium (IV) precursor is the first step in the sol-gel process. This is followed by polycondensation, which creates a colloidal solution or sol of hydroxide particles that are no larger than a few tens of nanometers. Ti-O-Ti bond formation is aided by a low water content (low hydrolysis) and an abundance of titanium alkoxide in the reaction mixture. A nearly organized three-dimensional polymer skeleton was formed as a result of chain creation. The rapid rate of hydrolysis hindered the growth of the Ti-O-Ti skeleton by encouraging the creation of Ti(OH)4. Loose packing of the particles is caused by many Ti-OH groups and inadequate formation of the three-dimensional structure of the polymer. Tetraisopropyl titanate was dissolved in isopropyl alcohol by Tran et al.and a mixed solution of isopropyl alcohol and water was gradually added. This process produces an amorphous TiO2 precursor via condensation and hydrolysis. It can be controlled by adjusting the reaction temperature, species, and acid concentration. Perego et al.immediately obtained BT through the thermal hydrolysis of TiCl3 and TiCl4 using the sol-gel technique. A standard preparation involved bringing the pH down to 4.5 using NaOH, and letting the particles remain at 60°C for a week without stirring.

The most homogeneous and environmentally friendly material is obtained by the sol-gel method, which is also an inexpensive method to obtain brookite. The disadvantages include a long synthesis period and the low crystallinity of the final products. Sol-gel is used to create nanoscale BT particles by hydrolyzing titanium precursors [73]. Titanium tetrachloride and titanium alkoxide were used as precursors. In the first step of the sol-gel process, the Ti(IV) precursor is hydrolyzed and then polycondensed, resulting in the formation of a colloidal solution, called sol, consisting of hydroxide particles that are less than a few tens of nanometers in size. The formation of the Ti-O-Ti bond was facilitated by the presence of a large amount of titanium alkoxide in the reaction mixture and a low concentration of water, which led to weak hydrolysis. As a result of chain formation, a three-dimensional almost ordered polymer framework was formed. At high hydrolysis rates, Ti(OH)4 was formed, which prevented the formation of the Ti-O-Ti skeleton. The poor packing of the particles is due to the abundance of Ti-OH groups and insufficient formation of the three-dimensional polymer framework [73,74].

2.3. Thermal Decomposition Method for the Synthesis of BT

Other ligands were added along with titanium ions during the synthesis process, and the concentration of the titanium precursor, anions/cations, and pH of the solution were adjusted to regulate the morphology and size of the brookite crystal phase. It has been reported that BT can be synthesized by simple thermal decomposition [75]. To obtain titanium oxalate hydrate ($Ti_2O_3(H_2O)_2(C_2O_4)\cdot H_2O$) by the precipitation method, a mixed solution of titanium oxide sulfate and oxalate precursor was refluxed and stirred at 90°C for various periods. Pure BT was then obtained using heat to destroy the $Ti_2O_3(H_2O)_2(C_2O_4)\cdot H_2O$ at 300-400°C, pure BT was obtained. First, in the synthesis process, amorphous bulk TiO2 aggregates were generated during the initial reflux reaction. Alkali metal ions (Li and Na) cause the bulk aggregate to disintegrate, forming a small-sized crystalline titanium oxalate hydrate. Ostwald aging causes the small-sized crystalline titanium oxalate hydrate to grow progressively larger when the reaction is sustained. The Ostwald aging effect eventually ended and the particle size started to progressively shrink. The different morphologies of titanium oxalate hydrate resulted from the evident variation in the adsorption ability of alkali ions on the crystal face of the material. Thermal destruction then formed the brookite phase of TiO2, which had a distinct shape, and it was found that its crystallinity increased with increasing temperature. They also described how different anions, such as Cl- and SO_4^{2-} affected the crystalline phase of TiO2, with Cl- being more favorable for the formation of the brookite phase. Then,

 doi:10.20944/preprints202501.1197.v1

by slightly modifying the procedure, anatase and brookite were obtained according to a previously described method for obtaining BT by thermal decomposition [76].

According to Pottier et al. [77], brookite nanoparticles were prepared by thermal breakdown in aqueous media without the need for a potent complexing agent (Figure 4). After aging, the crystalline phase of brookite was produced using the precursor Ti(OH)2(Cl)2(H2O)2 complex and TiCl4 was dipped in either strong hydrochloric acid or perchloric acid. As illustrated in Figure 4, the water-based ligand was first removed from the Ti(OH)2(Cl)2(H2O)2 precursor by condensation of water and hydroxyl ligands through hydroxylation. To obtain TiO2, hydroxyl groups and ligand chloride ions were further condensed by hydroxylation to eliminate HCl under thermal breakdown conditions. To obtain TiO2, hydroxyl groups and ligand chloride ions were further condensed by hydroxylation to eliminate HCl under thermal breakdown conditions.

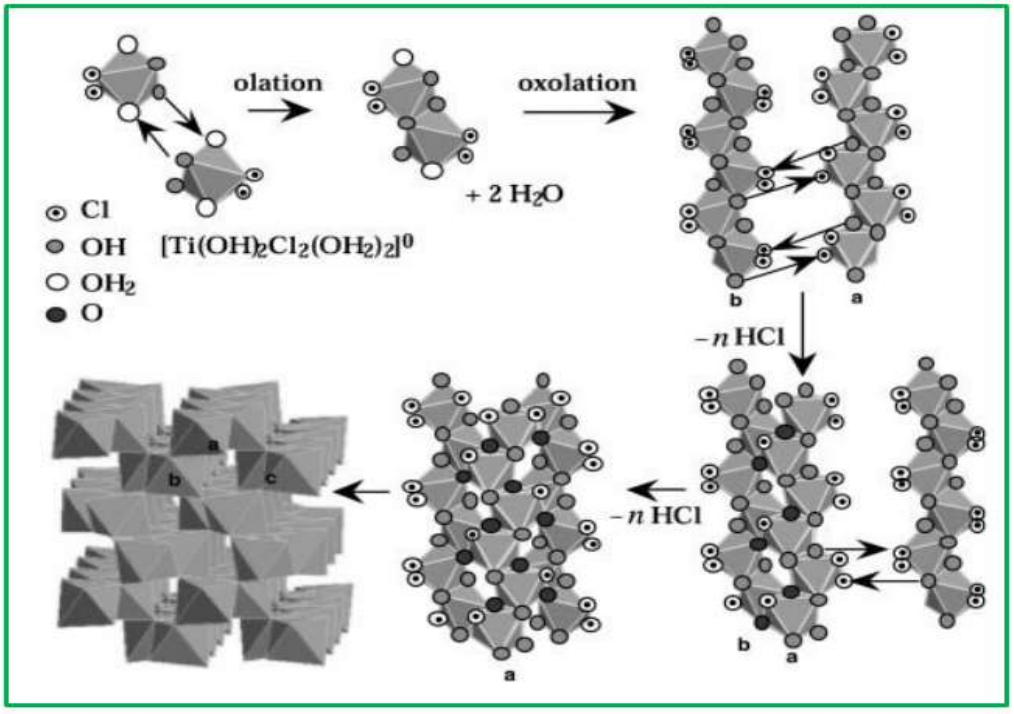

Figure 4. Possible Reaction Pathway for Brookite Formation from the [Ti(OH)2Cl2(OH2)2]0 Complex. Reproduced from Ref.with permission from American Chemical Society.

Among them, acidity and aging conditions were significant factors affecting the morphology of the brookite particles, and Cl- was a necessary condition to stabilize the formation of the brookite phase. The results for the TiO2 particles analyzed according to the scheme in Figure 4 are shown in Figure 5.

 doi:10.20944/preprints202501.1197.v1

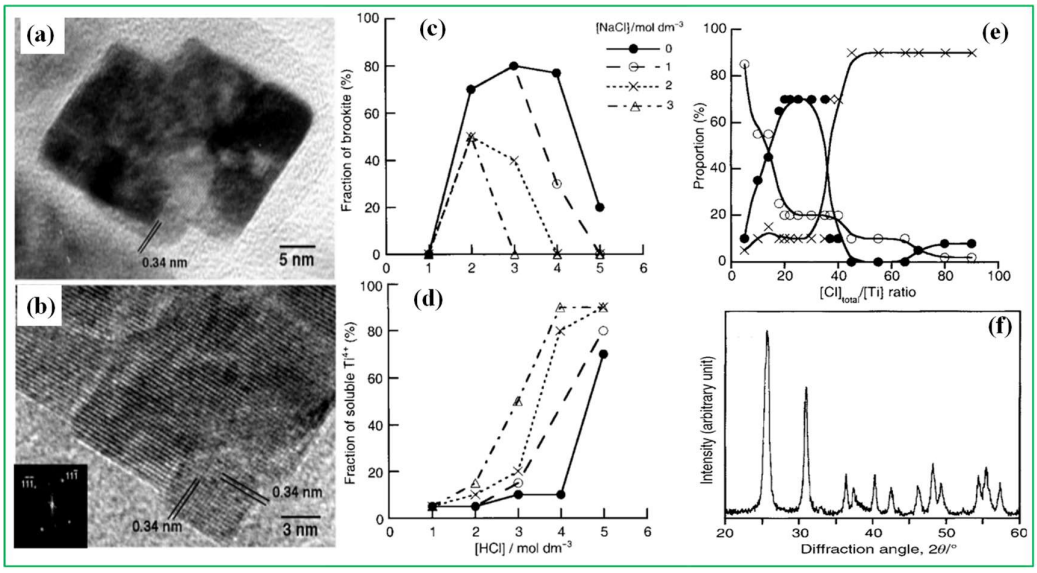

Figure 5. Micrographs and characteristics of TiO2 samples obtained by thermal decomposition: (A-B) HRTEM Micrographs of Brookite Particles Separated from Rutile by Peptization after One Month of Thermolysis at 100°C; (C) Fraction of Brookite in the Precipitate and Fraction of Soluble Titanium Moieties; (E) after 24h of Thermolysis on TiCl4 (0.15mol dm-3) in HCl Medium in the Presence of NaCl; (F) Ratio of Titanium in the Soluble Complex (×) and in the Solid State form (Brookite ● and rutile ○) as A Function of the Ratio of Cltotal:Ti after 24h of Thermolysis at 100°C for TiCl4; (F) X-ray Diffraction Patterns of Brookite Particles Resulting from Fractionation of the Precipitate Formed by Thermolysis of TiCl4 Solution. Reproduced from Ref.with permission from American Chemical Society.

The method developed by Buonsanti et al.for the high-temperature ammonolysis of titanium carboxylate complexes allowed the selective isolation of anisotropic TiO2 nanocrystals in the metastable brookite phase. TiCl4 was added to a solution containing oleylamine, oleic acid, and octadecene surfactants, as shown in [78], and the mixture was destroyed at 290°C. This process has been successfully applied by other groups to obtain BT [79]. TiO2 nanorods were created by introducing a standard molar amount of OLAC/TiCl4 mixture into the reaction system. A rod-like structure was observed in the resulting TiO2 brookite with 20mmol of TiCl4. TiO2 can be obtained and grown using this synthetic technique, and the obtained material has a predominantly anatase or brookite structure. Significant phase purity and BT can be produced using a straightforward algorithm; however, similar to the hydrothermal approach, this process has significant energy consumption and requires painstaking control over the feedstock shape.

2.4. Solvothermal Synthesis of BT

Except for the use of a non-aqueous solvent in the solvothermal method, the hydrothermal and solvothermal procedures are nearly identical. The solvothermal process can operate at substantially higher temperatures owing to the higher boiling points of certain organic solvents, the solvothermal process can operate at substantially higher temperatures [80]. Generally, the solvothermal process can be used to adjust the size, shape, and crystal structure of BT particles. This approach is a flexible strategy for creating several types of TiO2 with a limited dispersity and size distribution. It is possible to create TiO2 nanoparticles with a characteristic size of less than 5nm using the solvothermal approach [81,82]. However, this method has several drawbacks, including the inability to control contaminants, product shape, and size. However, this method is prima facie known in terms of ease of operation, high scalability, and low cost of obtaining brookite.

 doi:10.20944/preprints202501.1197.v1

To conclude this chapter, it should be noted that, despite the modern techniques developed, researchers face three main problems: firstly, obtaining pure brookite phase is a difficult task. Second, pure BT is not photocatalytically active in the absence of co-catalysts or structural modifications of the dopant. Third, since BT is metastable and transforms into rutile at high temperatures, it is difficult to obtain a pure brookite phase, unlike a combination containing titanium or anatase phase. However, literature review has shown that the hydrothermal reaction temperature, electrolyte concentration, pH, reaction duration, sample size and crystalline phase can be varied with various additives to solve this problem. In general, the shape and reaction process of BT can be controlled by hydrothermal technology, which is considered one of the simplest ways to produce this material.

3. ENHANCEMENT OF CO2 PHOTOREDUCTION BY MODIFICATION OF BT

The limitations of photocatalytic CO2 reduction can be overcome using BT modified in various ways. To achieve heterojunctions, various engineering techniques such as fitting crystal faces, attracting heteroatoms, loading of co-catalysts, and interaction with other phases of TiO2 or semiconductors are discussed herein. Table 1 provides an overview of the various modification methods and the associated photocatalytic efficiency of CO2 reduction by BT photocatalysts.

Table 1. Performance of Photocatalytic CO2 Reduction Using BT with Different Modifiers Obtained by Hydrothermal Method.

Materials	Light Source	Performance (μmol·h-1·g-1)	Strategies for CO2 Photoreduction Promotion	Reaction Medium	Reduction Products	Ref.
Pure TiO2	365nm light-emitting diode, 0.3mW/cm2	1.17	Crystal facet regulation	0.2M KHCO3 aqueous solution	CH3OH	[83]
Cu - TiO2	300W Xe-lamp	17.81 4.23	Schottky junctions	H2O vapor and CO2	CH4 CO	[84]
Ti3+ - TiO2-x	≥420nm visible light, 300W Xe lamp, 0.216W/cm2	11.9 23.5	Ti3+ defects enhances the visible light absorption and narrows the bandgap	H2O vapor and CO2	CH4 CO	[85]
Anatase/brookite	Solar simulator, 200-1,000nm, 69.6mW/cm2	2.1	Phase junction facilitates interfasial electron transport	H2O vapor and CO2	CO	[86]
Ag/MnOx - TiO2	300W Xe-lamp	129.98 31.70	Ag/MnOx nanoparticles serve as electron/hole sinks, and improve the adsorption/activation	H2O vapor and CO2	CH4 CO	[87]
Pt-TiO2/C3N4	300W Xe-lamp	31.8 3.8	p-n heterojunction	H2O vapor and CO2	CH4 CO	[88]

 doi:10.20944/preprints202501.1197.v1

SrCO3 - anatase/brookite	300W Xe-lamp	19.66 2.64	SrCO3 species improve the CO2 adsorption and activation abilities	H2O vapor and CO2	CH4 CO	[89]
NH2 - TiO2 - CuxS	300W Xe-lamp	3.34	p-n heterojunction	H2O vapor and CO2	CH4	[89]
NH2-B-TiO2/Cu	300W Xe-lamp	2.39 1.97	p-n heterojunction	H2O vapor	CH4 CO	[90]
NH2-B-TiO2/Ag	300W Xe-lamp	9.26	p-n heterojunction	H2O vapor	CH4	[90]
NH2-B-TiO2/Ni(OH)2	300W Xe-lamp	1.26 0.15	p-n heterojunction	H2O vapor	CH4 CO	[90]

Table 1 shows that the photocatalytic activity of modified BT is almost always higher than that of pure BT, and the photoreduction product is usually CH4CO. The following is a list of known methods for improving photocatalysis that can be used with BT.

3.1. Optimization of Photocatalytic Activity of BT by Tailoring Crystal Faces

One promising way to increase the catalytic activity of TiO2 is to tune the crystalline faces of the brookite phase, which can be achieved by adjusting the synthesis conditions. Through the hydrothermal treatment of a titanium precursor in the presence of PVA or PVP, Ohno et al.created BT nanorods with particular crystal faces. The reducing center was located on the {2 1 0} crystal face and the oxidation center was located on the {2 1 2} crystal face. Pt and PbO2 were loaded as reduction and oxidation sites, respectively, on the distinct crystal faces of brookite. Owing to the separation of the redox centers, the photocatalytic reduction activity of CO2 was higher than that of the commercial spherical BT, and the multi-electron reduction ability was enhanced. The primary result of the CO2 reduction to CH3OH using the obtained BT as a photocatalyst without a co-catalyst is shown in Figure 6.

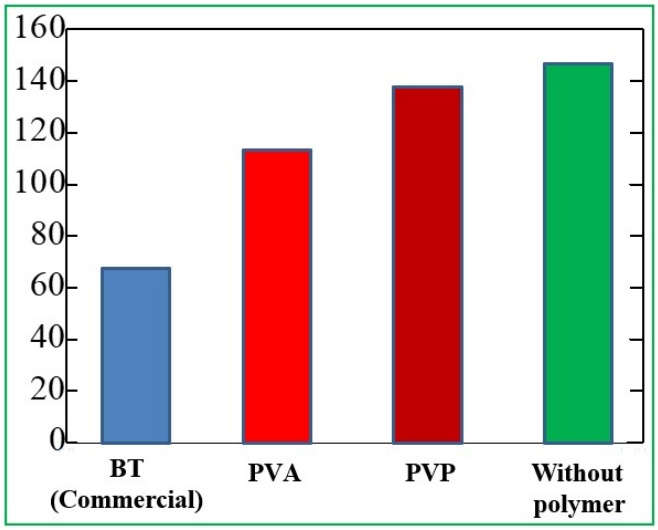

Figure 6. Diagram of Photocatalytic Activity of BT, PVA and PVP Nanorods Without Polymer. The diagram was redrawn from Ref. [84].

 doi:10.20944/preprints202501.1197.v1

The results demonstrated that commercial BT had lower CO2 reduction activity than BT, with a high elongation ratio of two nanorods with an open crystal phase. Stated differently, it is crucial to enhance the photocatalytic CO2 reduction activity by expanding the {2 1 0} crystal plane reduction site, even if the co-catalyst particle size and aggregation state greatly impact the selectivity of CH3OH generation.

3.2. Effect of Metal Ion Doping on the Photocatalytic Activity of BT

The electrical structure of a semiconductor can be modified by doping it with metals or nonmetals. This can affect the optical absorption and transport of photoinduced electron-hole pairs, which is crucial for the subsequent photocatalysis process. This is one of the most commonly used methods for modifying semiconductors to improve their photocatalytic efficiency. It has been reported that a hydrothermal approach based on surface oxidation has been used to obtain single-crystalline Ti3+ self-alloyed BT nanosheets [86]. Figure 7A and 7B show the SEM and TEM images of the obtained samples, respectively.

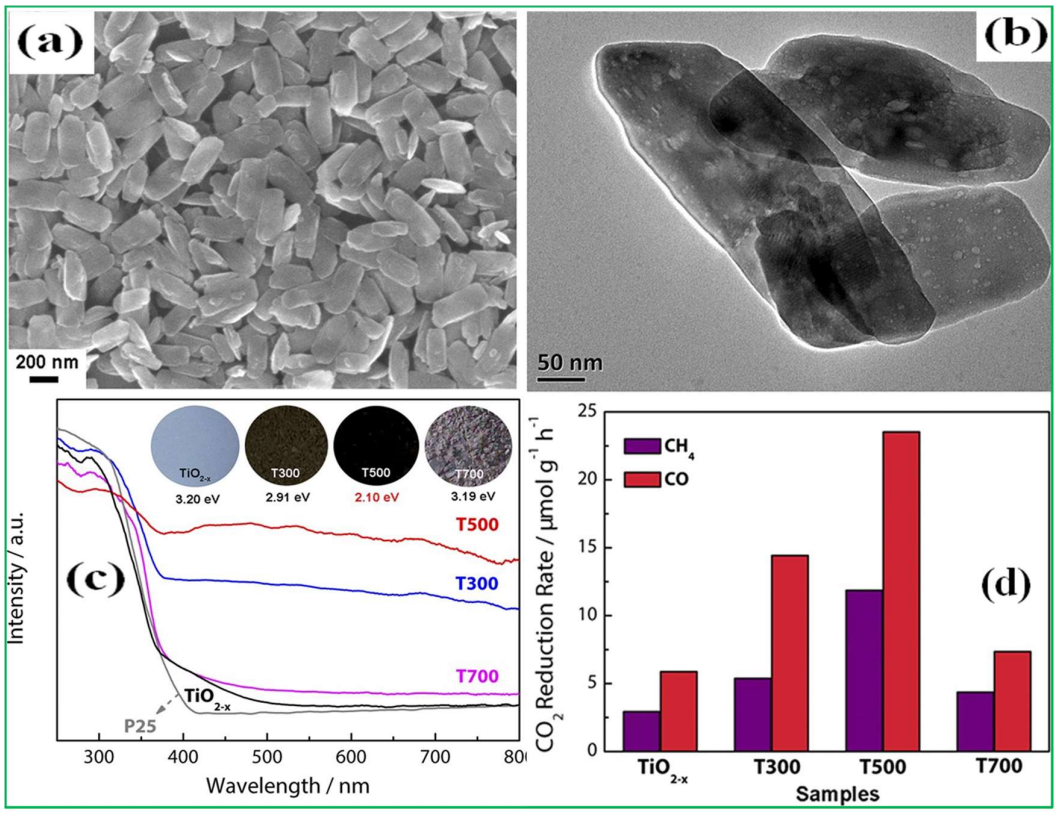

Figure 7. SEM/TEM Analysis and Evaluation of Photocatalytic Activity of Ti3+ Self-alloyed BT Samples: (A) SEM and (B) TEM Images of Ti3+ Self-alloyed BT Samples; (C) UV-visible Diffuse Reflectance Spectra; (D) CO2 Photoreduction Rate of TiO2-x, Samples T300, T500 and T700. Reproduced from Ref.with Permission from Springer Nature Ltd.

This synthesis approach is gentle and simple compared to other complex and expensive physical methods, such as high-temperature pressurized hydrogenation and plasma treatment. By annealing at different temperatures, TiO2 nanosheets with a tunable number of Ti3+ defects can be obtained by self-alloying with Ti3+ brookite TiO2. As shown in Figure 7C, the color of ideal nanocrystalline TiO2

 doi:10.20944/preprints202501.1197.v1

with Ti3+ defects was dramatically different from that of white TiO2, and the absorption range of BT with Ti3+ defects significantly increased. Without annealing, the activity of self-alloyed Ti3+ brookite was low, as shown in Figure 7D. The CO2 reduction rate reached its maximum at a calcination temperature of 500°C.

3.3. Loading of Co-catalyst in BT

It is well-known that the surface catalytic ability of BT is insufficient. One of the most effective ways to solve this problem is the addition of co-catalysts to the BT surface. The authorseffectively loaded Ag nanoparticles on BT by a chemical reduction method after adding AgNO3 and NaBH4 solution to the native BT. The selectivity for CO2 reduction is discussed in detail in this study. The size of the TiO2 brookite and the loading of Ag on the different exposed crystal surfaces significantly influenced the activity and selectivity of CO2 photoreduction from CO/CH4. The selectivity of CO2 and its intermediates, such as $C0_3^{2-}$, HCO3- and other carbonates, is directly correlated with the adsorption of CO2. Figure 8 shows the composition and crystal phase of the prepared samples supplemented with single or double cocatalysts. The maximum reducing activity was observed at a Ag dosage of 0.5% CO2, as shown in Figure 8A and 8B. At a relatively low Ag loading, as shown in Figure 8C, Ag nanoparticles were mainly distributed on the {2 1 0} crystal plane, and CO2 was mainly converted into CO. When the Ag dosage is too high, the redox activity of CO2 is very low. Transition metals/metal oxides are preferred co-catalysts in low-cost photocatalytic applications over noble metals (such as Pt, Ag, and Rh) [91,92]. Cu-TiO2 synthesized in Ref.demonstrated excellent photocatalytic activity and selectivity for CO2/CH4 photoreduction compared with the chemical reduction approach. This was mainly caused by the adsorption of CO2/H2O Cu-brookite onto TiO2 and the varying amounts of unoccupied surface oxygen. The effect of dual cocatalysts on the photocatalytic CO2 reduction of BT was further studied by Xiao et al [94].

Based on these data, the Ag/Mn species that decorate BT appear to have a very low crystallinity and real load content. The Ti/O molar ratios of pure TiO2 and its composites are generally comparable to the expected stoichiometric ratio (1:2) of dioxide. The results of elemental analysis also showed the presence of Ag/Mn species in the TiO2-based composites (Table 2).

Table 2. Elemental Composition of Pristine Brookite Titanium Dioxide (BT) and its Typical Composites [94].

Sample	Ti (wt%)	O (wt%)	Ag (wt%)a	Mn (wt%)a
BT	59.90	40.10	-	-
0.5Ag- BT	59.56	40.00	0.44 (88%)	-
1.0Ag- BT	59.33	39.78	0.89 (89%)	-
BT -0.5Mn	59.65	40.12	-	0.23 (46%)
BT-1.0Mn	59.39	40.13	-	0.48 (48%)
0.5Ag- BT -0.1Mn	59.64	39.85	0.43 (86%)	0.08 (80%)
0.5Ag- BT -0.2Mn	59.42	39.97	0.44 (88%)	0.17 (85%)
0.5Ag- BT -0.5Mn	59.12	39.99	0.45 (90%)	0.44 (88%)
0.5 Ag- BT -1.0Mn	58.81	39.85	0.45 (90%)	0.89(89%)

The observed weight ratio of Ag species in the xAg-BT and 0.5Ag-BT-yMn composites was only marginally less than the equivalent added content, indicating that the majority of the added Ag

 doi:10.20944/preprints202501.1197.v1

species could be reduced and utilized as Ag metal nanoparticles to adorn the TiO2 surface. A degree of loss (up to 50%) of Mn content was observed in comparison with the theoretical added amounts (0.5 and 1.0%) of Mn particles. This suggests that the photooxidation of Mn2+ ions was inadequate because, as previously noted, an acceptable electron capture reagent was not present.

The 0.5Ag-BT-yMn composites have a rather high Mn content because Ag species are utilized to adorn the BT nanoparticles. These findings are in line with the preceding X-ray photoelectron spectroscopy (XPS) results and imply that Ag loading is beneficial for the creation and ornamentation of MnOx on BT. For instance, the measured Mn content (0.23wt%) in the BT-0.5Mn composite is equal to 46% of its theoretical composition, whereas the measured Ag and Mn contents (0.45 and 0.44wt%) in the 0.5Ag-BT-0.5Mn composite are 90 and 88% of their theoretical additions, respectively (Table 2). These data demonstrate that Ag and MnOx nanoparticles can be used to successfully adorn BT nanoparticles; however, given the current deposition conditions, Ag nanoparticles are more effective at decorating the BT surface than MnOx nanoparticles.

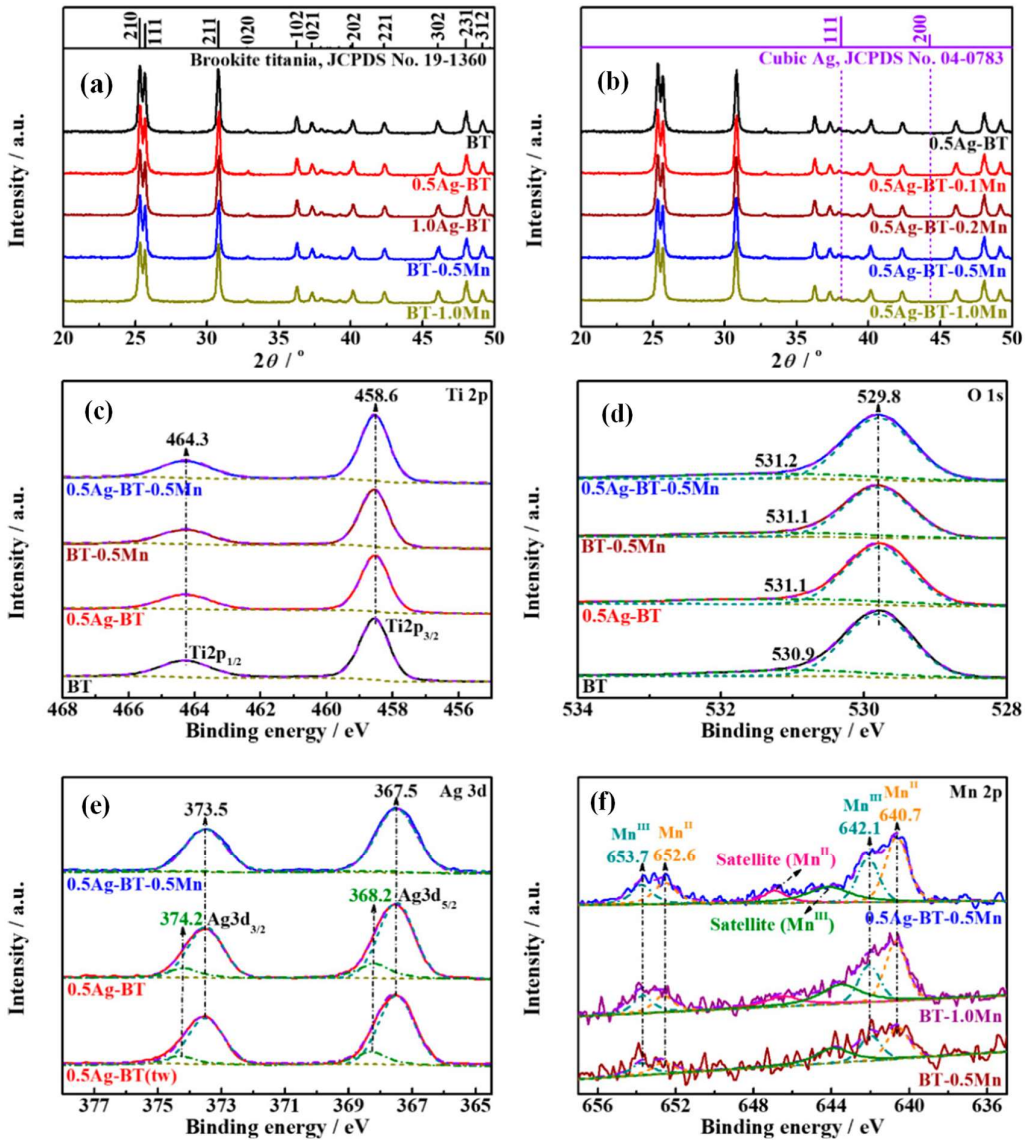

Figure 8. Analysis of the influence of co-catalysts on the structure and properties of BT using XRD and XPS methods. A: Typical X-ray Diffractometers of Primordial BT and its Composites (xAg-BT and BTN-yMn). B: Typical x-ray Diffraction Patterns of Composites 0.5Ag-BTN-yMn; C: High Resolution XPS Spectres of Ti2p; D:

 doi:10.20944/preprints202501.1197.v1

High Resolution XPS Spectres of O1s; E: High Resolution XPS Spectres of Ag3d; F: High Resolution XPS Spectres of Mn2p for Primary BT and its Typical Composites (0.5Ag-BT, BT-0.5Mn/5G). Reproduced from Ref.with Permission from American Chemical Society.

Nonetheless, the X-ray photoelectron spectra published by the authors showed that Ag and Mn were both successfully used to decorate brookite nanoparticles during the photodeposition process, as these composites, 0.5Ag-BT, BT-0.5Mn, and 0.5Ag-BT-0.5Mn, display signals of Ag and/or Mn species in addition to random carbon and binding energy peaks of Ti and O (Figure 9).

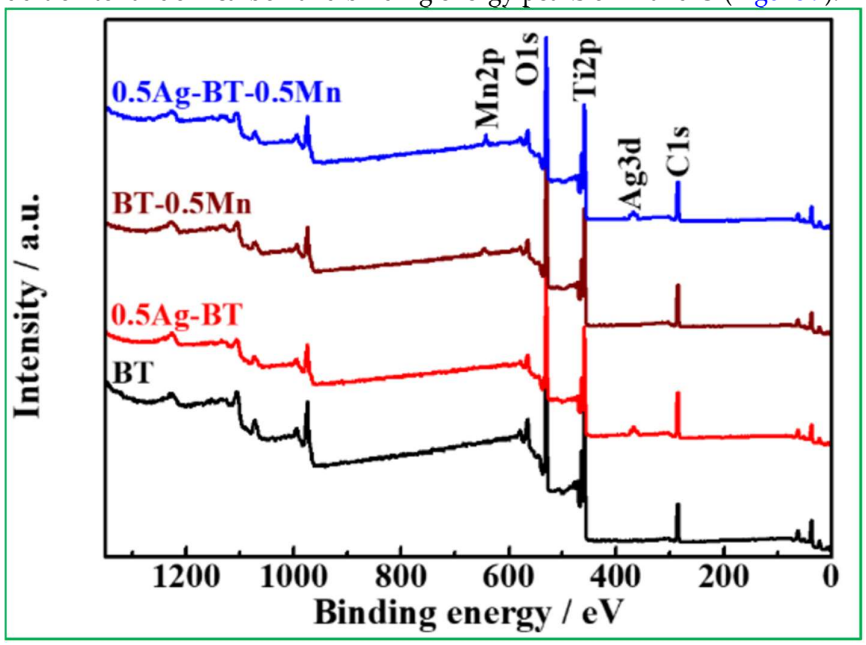

Figure 9. Survey XPS Spectra of the Pristine BT and its Typical Composites (0.5Ag-BT, BT-0.5Mn and 0.5Ag-BT-0.5Mn). Reproduced from Ref.with Permission from American Chemical Society.

Figure 8A illustrates that the XRD pattern of the hydrothermally produced product closely matches the standard map of BT (JCPDS no. 29-1360). Because rutile or anatase titanium does not exhibit any noticeable reflection signal, it is likely that the result of hydrothermal synthesis is brookite titanium dioxide with high phase purity. The XRD patterns of the resulting composites loaded with a single cocatalyst (xAg-BT and BT-yMn) were extremely similar to those of pure BT after loading with Ag or Mn particles, and there was no noticeable silver/manganese metal reflectance signal or their oxides were visible (Figure 8A). As for the composites supplemented with dual cocatalyst (0.5Ag-BT-yMn) and 0.5wt% silver content, the XRD pattern also perfectly matches brookite titanium (JCPDS no. 29-1360) and silver/manganese metals or their oxides are clearly visible (Figure 8B).

The high-resolution XPS spectra of Ti2p of pristine BT and its composites show the same two peaks at 458.6 and 464.3eV (Figure 8C) which indicates that the chemical state of Ti(IV) in brookite titanium does not change after the photodeposition process [88,95]. Two Gaussian components at 529.8 and 530.9eV (Figure 8D) can be primarily fitted to the high-resolution spectra of O 1s for the pure BT. These components are associated with the oxygen of the surface − OH groups of titanium and their lattice oxygen, respectively [88,96]. The oxygen lattice peak (529.8eV) in the 0.5Ag-BT, BT-0.5Mn, and 0.5Ag-BT-0.5Mn composites was identical to that of pristine BT. It is assumed that Ag and Mn were not doped into the crystal lattice; rather, they decorated the surface of the BT nanoparticles, as evidenced by the similar chemical states of Ti(IV) and Ti lattice oxygen for these samples. In the high-resolution spectrum Ag3d (Figure 8E) of the 0.5Ag-BT composite, two groups

 doi:10.20944/preprints202501.1197.v1

of peaks can be distinguished: Ag(I) species are represented by relatively weaker peaks located at levels 368.2 (3d5/2) and 374.2 (3d3/2)eV, and the stronger peaks at 367.5 (3d5/2) and 373.5 (3d3/2)eV are attributed to the metal forms of Ag [97]. This indicates that very few Ag(I) particles coexist with the metal composite coated with Ag nanoparticles and that these particles cannot be photoreduced by the photodeposition process. Nevertheless, the high-resolution XPS spectra of Ag3d for the 0.5Ag-BT-0.5Mn composite showed no discernible Ag(I) signal (Figure 8E). These findings imply that, for the 0.5Ag-BT-0.5Mn composite, the longer photoreduction duration used to prepare the 0.5Ag-BT-yMn composite cannot cause the Ag(I) species to vanish, but the additional Mn2+ ions in the solution photodeposition can successfully encourage the photoreduction of Ag ions by absorbing holes created by BT.

The high-resolution XPS spectra of Mn 2p for the 0.5Ag-BT-0.5Mn composite can be deconvoluted into two Gaussian components at 640.7/652.6 and 642.1/653.7eV, which can be assigned to Mn(II)2p3/2/Mn(II)2p3/2 and Mn(III)2p1/2/Mn(III)2p1/2, respectively [98–100]. These results indicate that mixed valence states of Mn(II)/Mn(III) species (hereafter referred to as MnOx) exist in Mn-containing composites [100]. However, the BT-0.5Mn composite exhibited very weak Mn2p signals, implying a very low actual load magnitude. A possible reason may be that the photooxidation of Mn2+ ions is difficult due to the lack of an electron capture reagent when only Mn2+ ions are added to the BT suspension during the precipitation process. In other words, by absorbing the photoinduced BT electrons, the Ag ions introduced initially to the photodeposition solution will encourage the photooxidation of the Mn2+ ions, which will later be added together with the remaining photoinduced holes. Consequently, compared to BT-0.5Mn, the Mn2p peaks of 0.5Ag-BT-0.5Mn were substantially stronger. The BT-1.0Mn composite, which has a theoretical Mn content of 1.0 weight percent, displays a substantially brighter Mn2p XPS spectrum than the BT-0.5Mn composite, which lends more credence to this theory (Figure 8F). According to the aforementioned findings, Ag species are primarily found in metallic Ag nanoparticles, whereas Mn species are primarily found in MnOx with Mn(II)/Mn(III) valence states in BT-based composites.

The results show that a straightforward photodeposition technique is effective for producing Ag/MnOx supported BT. The photocatalytic CO2 reduction activity and CH4 selectivity are significantly enhanced. The photoluminescence spectra of the samples demonstrated that the BT-based Ag/MnOx binary cocatalysts could more successfully prevent photogenerated electrons and holes from recombining. The in-situ drift spectra under both light and dark conditions are shown in Figure 10.

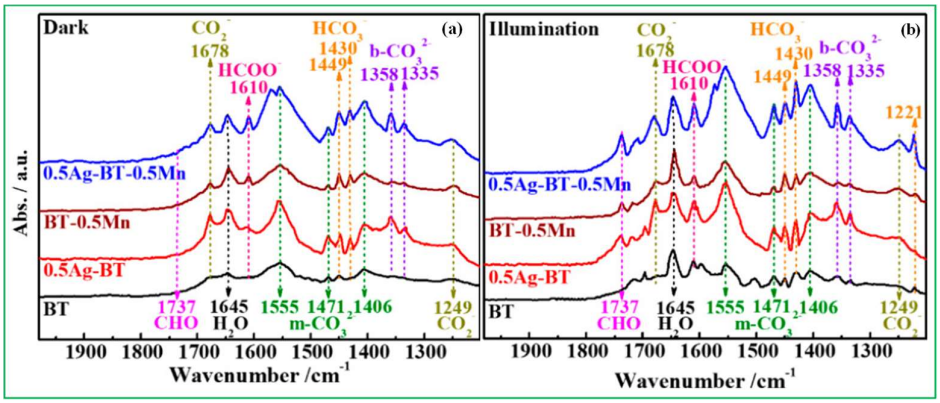

Figure 10. In Situ DRIFT Spectra of CO2/H2O Pair on Pristine BT and its Typical Composites. A: In the Dark; B: Under Illumination for 20min for the Entire Spectrum of Xe Lamps. Reproduced from Ref.with Permission from American Chemical Society.

 doi:10.20944/preprints202501.1197.v1

The BT-0.5Mn composite exhibited a drift spectrum in situ that was comparable to that of the 0.5Ag-BT composite (Figure 10A), but the adsorbed CO2/H2O molecules clearly showed lower signals. This suggests that the CO2/H2O adsorption capacity of the composite BT-0.5Mn was lower than that of its product decorated with Ag in the dark. According to these findings, Ag/MnOx Double Co-atalizers can be employed as holes and electron scavengers to separate photogenerated electrons and holes. MnOx can be used as a hole scavenger for hole traps, and Ag can be used as an electron scavenger for electron capture.

More significantly, it can alter the surface characteristics of BT nanoparticles, enhancing CO2/H2O adsorption or activation capability, and enhancing CH4 selectivity. The amplification of the signal of these infrared absorptions reaches a maximum (at 1.555/1.471/1,406, 1.449/1.430/1,221, and 1.358/1.335cm-1) for the composite 0.5Ag-BT after loading with Ag nanoparticles and was more noticeable than for the original BT after illumination. One possible explanation for the higher CO2RR capacity of the Ag-decorated composite is the chemicals produced by the 0.5Ag-BT composite during lighting. Further evidence that BT composites decorated with Ag provide increased CO generation activity may be due to the composite 0.5Ag-BT after lighting (Figure 10B), which exhibits more prominent and stronger IR peaks at a distance of 1.358/1.335cm-1 for CO_3^{2-} (which promotes CO2 formation) than a single BT under darkness or light (Figure 10).

3.4. Effect of Single/Double Cocatalyst on BT Photoactivity

Experiments have demonstrated that CO/CH4, which is the primary reducing product, originates from the photoreaction of CO2/H2O rather than from the breakdown of another material in the photocatalyst, as indicated in Section 3.3. Clean BT exhibited a CO/CH4 production of 20.55/6.37μmol·g-1·h-1, as shown in Figure 11A. The CO2RR increased quickly upon loading with Ag nanoparticles and then decreased slightly when excess Ag nanoparticles were loaded. The 0.5Ag-BT composite CO/CH4 output is the highest, measuring 61.50/83.46 μmol·g-1·h-1 with a total photoactivity of 790.68 μmol·g-1·h-1, which is 8.58 times higher than a single BT [94].

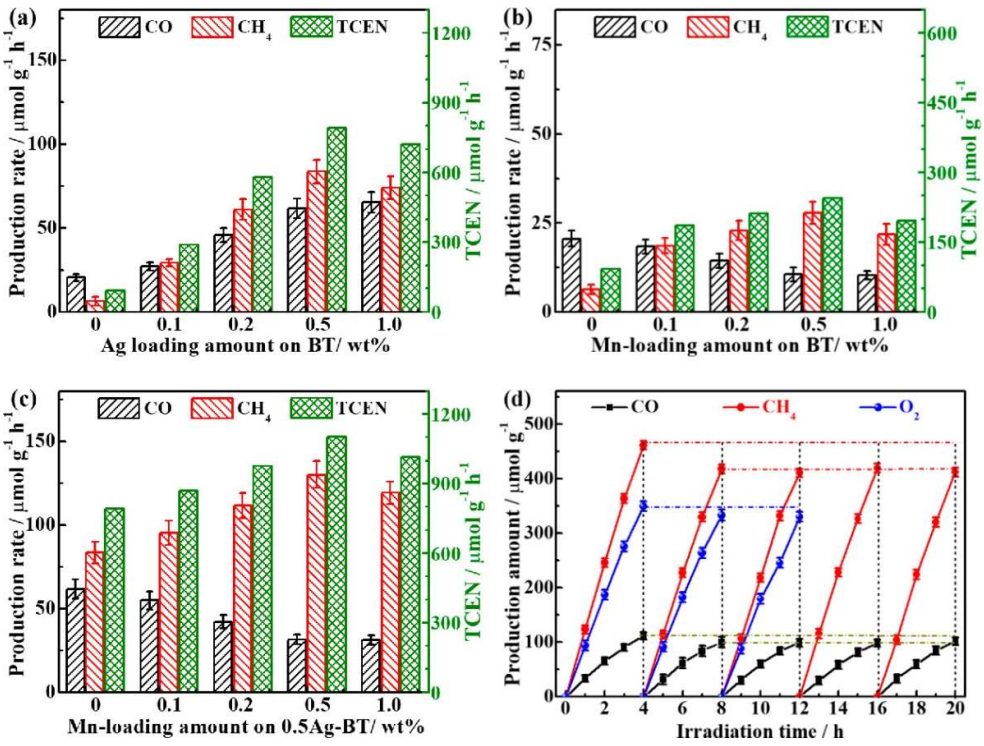

 doi:10.20944/preprints202501.1197.v1

Figure 11. The influence of cocatalytic materials on the photocatalytic activity of BT: (A) Influence of Ag and B: Influence of Mn on Photocatalytic CO2RR Activity of Obtained Nanoparticles BT; (C) Influence of Loading Concentration Mn on Photocatalytic CO2RR Activity of Composite 0,5Ag-BT; (D) Photostability of Photocatalytic CO2 Composite 0,5Ag-BT-0,5Mn. Reproduced from Ref.with Permission from American Chemical Society.

The composite 0.5Mn-BT exhibits the best CO/CH4 production (10.58/27.85μmol·g-1·h-1 with a total photoactivity of 243.96μmol·g-1·h-1) 2.65 times greater than BT alone. However, the CO2RR improvement with MnOx nanoparticles was quite weak (Figure 11B). These findings indicate that BT nanoparticles decorated with Ag and MnOx nanoparticles may both increase CO2RR; however, the stimulating effect of Ag nanoparticles is evidently greater than that of MnOx nanoparticles. It is possible to determine that the CH4 composite selectivity of BT-0.5Mn is up to 72.5% based on the corresponding product selectivity, which is defined as the output percentage of a particular reduced product relative to the total output of all reduced products. This is significantly higher than that of the original BT composite (23.7%) and composite 0.5Ag-BT (57.6%), indicating that MnOx species on BT are more favorable for CH4 production.

The dual co-catalyst composites provided higher productivity for CO2RR compared to the single co-catalyst composites (xAg-BT and BT-yMn). With a yield of 31.70/129.98μmol·g-1·h-1, the 0.5Ag-BT-0.5Mn composite exhibits the highest CO/CH4 activity among them (Figure 11C). The corresponding total photoactivity can reach 1103.28μmol·g-1·h-1, which was 11.98, 1.39 and 4.52 times higher than those of pure BT, 0.5Ag-BT, and BT-0.5Mn samples, respectively. In addition, 0.5Ag-BT-0.5Mn exhibited much higher selectivity for the CH4 product (80.4%) than the 0.5Ag-BT (57.6%) and BT-0.5Mn (72.5%) composites. The significantly better CO2RR performance of the 0.5Ag-BT-0.5Mn composite was the result of the synergistic action of the Ag/MnOx dual catalysts on the BT nanoparticles. Apparent quantum yield (AQY), defined as the molar percentage of the number of electrons consumed by reduced products, in relation to the number of incident photons [101,102], can be calculated as 2.25% for composite take 0.5Ag-BT-0.5Mn with CO/CH4 output level 31.70/129.98μmol·g-1·h-1 (Figure 11B). The output of CO/CH4 (31.7/129.98μmol·g-1·h-1) and AQY (2.25%) of the composite is 0.5Ag-BT-0.5Mn better than that of the majority of BT-based catalysts reported recently, according to a comparison of the performance of CO2RR based on TiO2 photocatalysts previously reported [101–103]. Furthermore, by employing the same procedure to replace BT nanoparticles used to decorate Ag and MnOx with commercial TiO2 (P25, Degussa) or homemade γ-Al2O3 nanoparticles, the resultant 0.5Ag-P25-0.5Mn merely offers CO/CH4 output closer to 23.52/58.26μmol·g-1·h-1 and CH4 selectivity 71.2%, which is significantly lower than 0.5Ag-BT-0.5Mn. Furthermore, there was no visible photoactivity in 0.5Ag-Al2O3-0.5Mn. These findings demonstrate that photoactive TiO2 is essential for photocatalytic CO2 production and that its photoactivity is highly dependent on its microstructure and constituents. Specifically, the synergistic effect of the two BT counteratalizers on the nanoparticles causes a notable increase in the CO2RR concentration, offering a straightforward yet widely used method for producing a high-performance TiO2-based CO2RR photocatalyst.

3.5. Photocatalytic Reduction of CO2 Using Mixed TiO2

One of the main sources of greenhouse effects leading to global warming is CO2. However, CO2 is also a viable source of carbon as it can be converted into a number of valuable fuels and chemical compounds, including CH4, CH3 OH, and HCOOH. In order to provide a sustainable energy future while reducing CO2 emissions, new materials and technologies have been created to convert CO2. Solar-activated photocatalytic CO2 reduction using TiO2 in water at ambient temperature and

 doi:10.20944/preprints202501.1197.v1

atmospheric pressure has attracted attention due to its "green chemistry" and relatively low cost, in addition to solar thermochemical conversion and electrochemical reduction methods. In the photoreduction process of CO2/H2O, electron-hole pairs are formed on the surface of the TiO2 catalyst under photo-illumination. CO2 can be reduced by excited electrons in the CB of TiO2 migrating to the surface. H2O can be converted to O2 in the intermediate state by holes still present in the VB of TiO2.

It has been shown that the type of TiO2 phase and photocatalytic process discussed above are closely related. In Ref. [104], three polymorphic varieties of TiO2 nanocrystals (anatase, rutile, and brookite) were used to study the photoreduction of CO2 using water vapor. According to the experimental data, the photocatalytic reduction activity is distributed as follows:

Brookite>Anatase>Rutile

Rutile is the least active mineral, mainly due to the rapid recombination of e- and h+. In addition, they studied the photoreduction behavior of helium-treated TiO2 catalysts. According to the photoreduction results, the helium-treated catalysts were more active than the untreated catalysts. In addition, according to Figure 12, the sequence of catalytic activities for CO and CH4 generation during CO2 photoreduction is as follows: brookite>anatase>rutile, with brookite showing the highest photocatalytic activity. According to the results of this study, the brookite phase is a promising for the reduction of CO2.

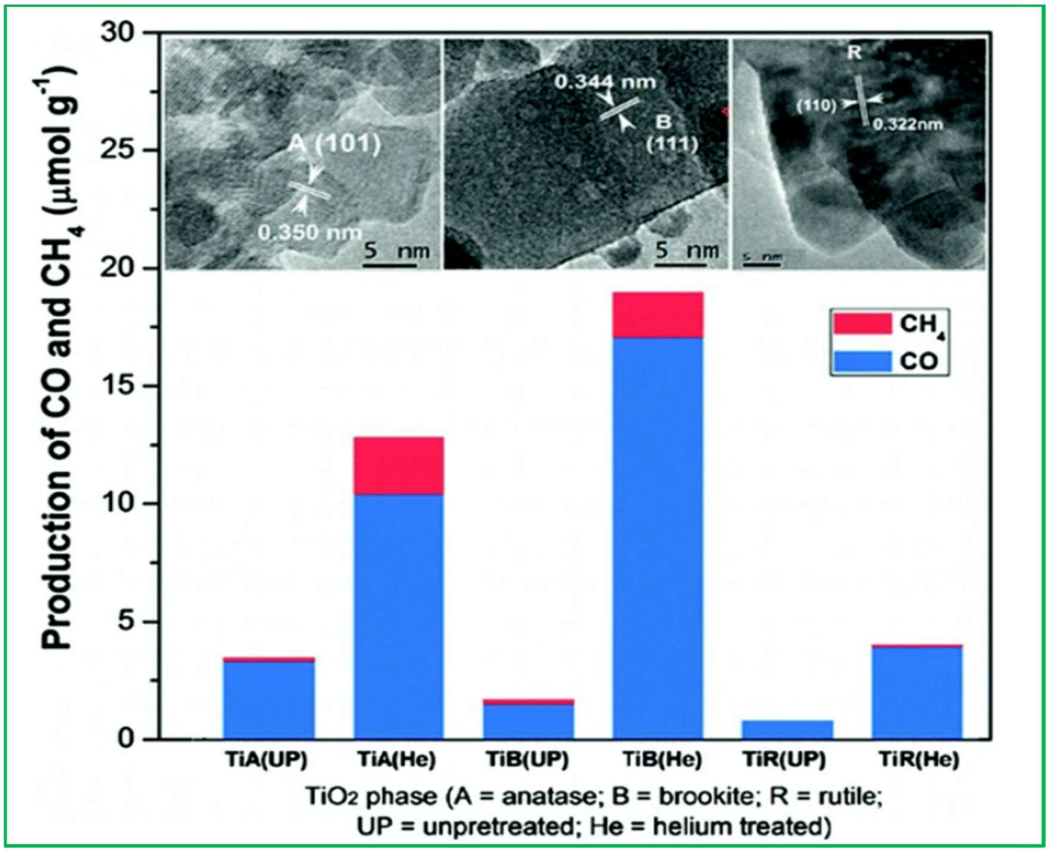

Figure 12. Results of TEM analysis of TiO2 polymorphs and Production of CO and CH4 based on them. The Upper Figures Represent the TEM Images of Anatase, Brookite and Rutile (From Left to Right). The Lower Figure Represents the Production of CO and CH4 in Three Different TiO2 Polymorphs. Reproduced from Ref.with Permission from American Chemical Society.

 doi:10.20944/preprints202501.1197.v1

Additional research on this subject was conducted by the authors, including an investigation of mixed phases containing brookite. A hydrothermal approach was used to create bicrystalline anatase/brookite TiO2 [105]. Additionally, CO2 was photoreduced in the presence of water vapor using freshly prepared bicrystalline TiO2 to produce CO and CH4. Commercial anatase/rutile TiO2 (P25), pure anatase, and pure brookite were used to compare their photocatalytic activities. According to the data shown in Figure 13, bicrystalline anatase/brookite was typically more active than pure anatase, brookite, and P25. With almost twice the photocatalytic activity of pure anatase (A100) and three times that of single-phase brookite, the bicrystalline combination consisting of 75% anatase and 25% brookite demonstrated the highest level of activity. It is suggested that the interaction between anatase and brookite nanocrystals is responsible for the enhanced activity of the bicrystalline anatase/brookite. Moreover, the anatase-rich bicrystalline anatase and brookite mixtures were superior to the anatase and rutile mixtures of P25, suggesting that the interaction between anatase and brookite with CO2 photoreduction is more efficient than the interaction between anatase and rutile (as in P25).

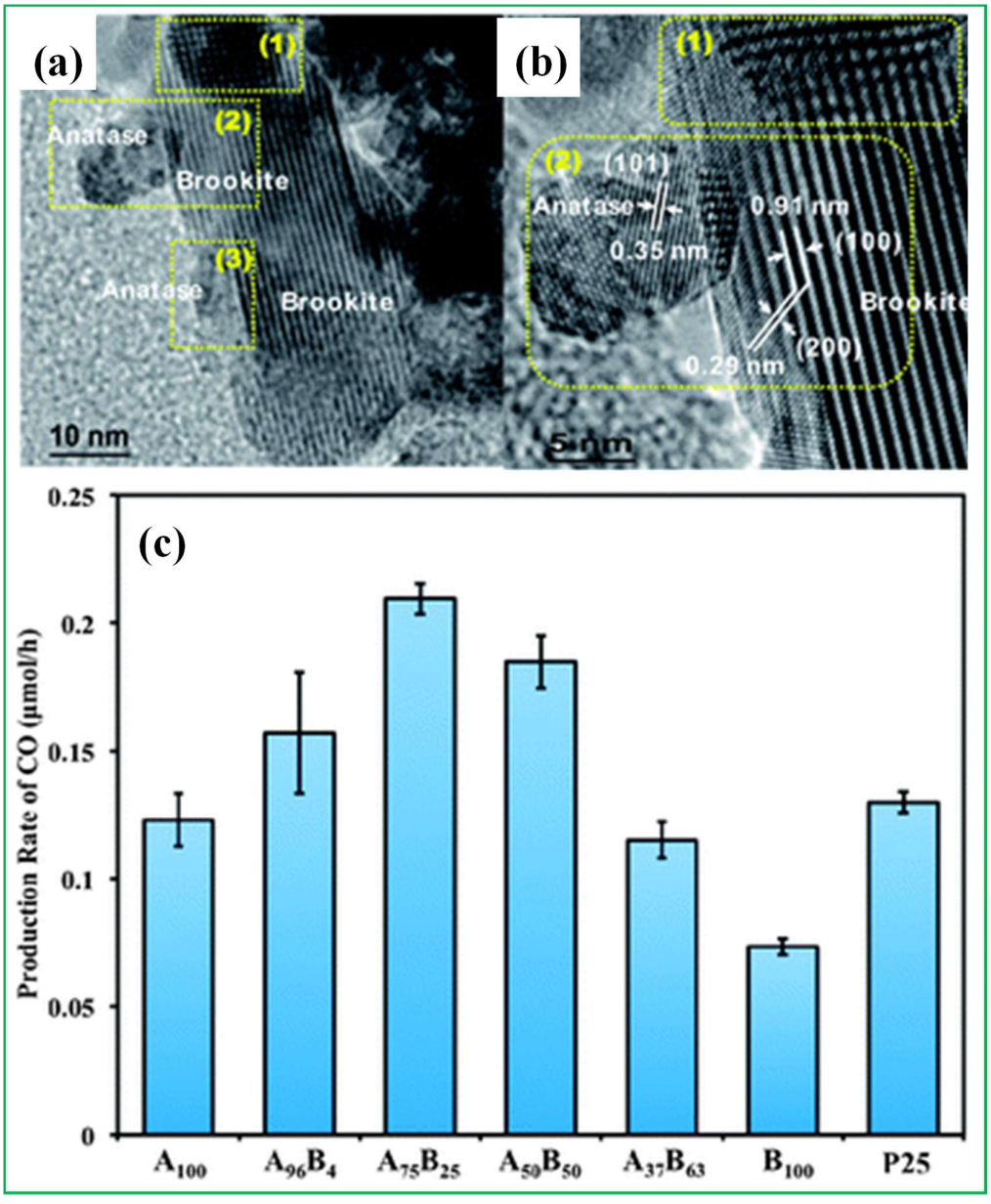

 doi:10.20944/preprints202501.1197.v1

Figure 13. Analysis of the morphology of TiO2 catalysts (anatase and brookite) and CO production based on them: (A) TEM and (B) HRTEM Images of Mixed Phase TiO2 with Anatase/Brookite ratio=75:25 (A75B25); (C) CO Production on Different TiO2 Catalysts (A=Anatase, B=Brookite, Subscript Numbers are Phase Fraction of Anatase and Brookite). Reproduced from Ref.with permission from the Royal Society of Chemistry.

Que et al.investigated a coexisting brookite/anatase/rutile TiO2 composite as a photocatalyst for the degradation of organic pollutants (Figure 14A). They found that in nanopowders composed of brookite/anatase/rutile, the rutile phase crystallizes into single-crystalline nanorods with a diameter of ~20nm and a size of 100-500nm in length, whereas the brookite phase crystallizes into irregular nanoparticles with a diameter of <20nm. It was shown that under UV light irradiation, the three-phase TiO2 catalyst exhibited higher photocatalytic activity for the cleavage of methyl orange (MO) than the two-phase commercial catalyst P25. The sample with the highest photocatalytic activity, designated T2, contained 29.9% anatase, 27.9% brookite, and 42.2% rutile. This sample bleached more than 90% of the MO solution in only 20min (Figure 14B). Furthermore, as shown in Figure 14C, photocatalyst recycling studies were conducted using the best TiO2 photocatalyst sample. It is evident that following five recycling cycles, the sample's photocatalytic activity only marginally drops, suggesting that the three-phase TiO2 catalyst exhibits high stability during the photocatalytic degradation process.

 doi:10.20944/preprints202501.1197.v1

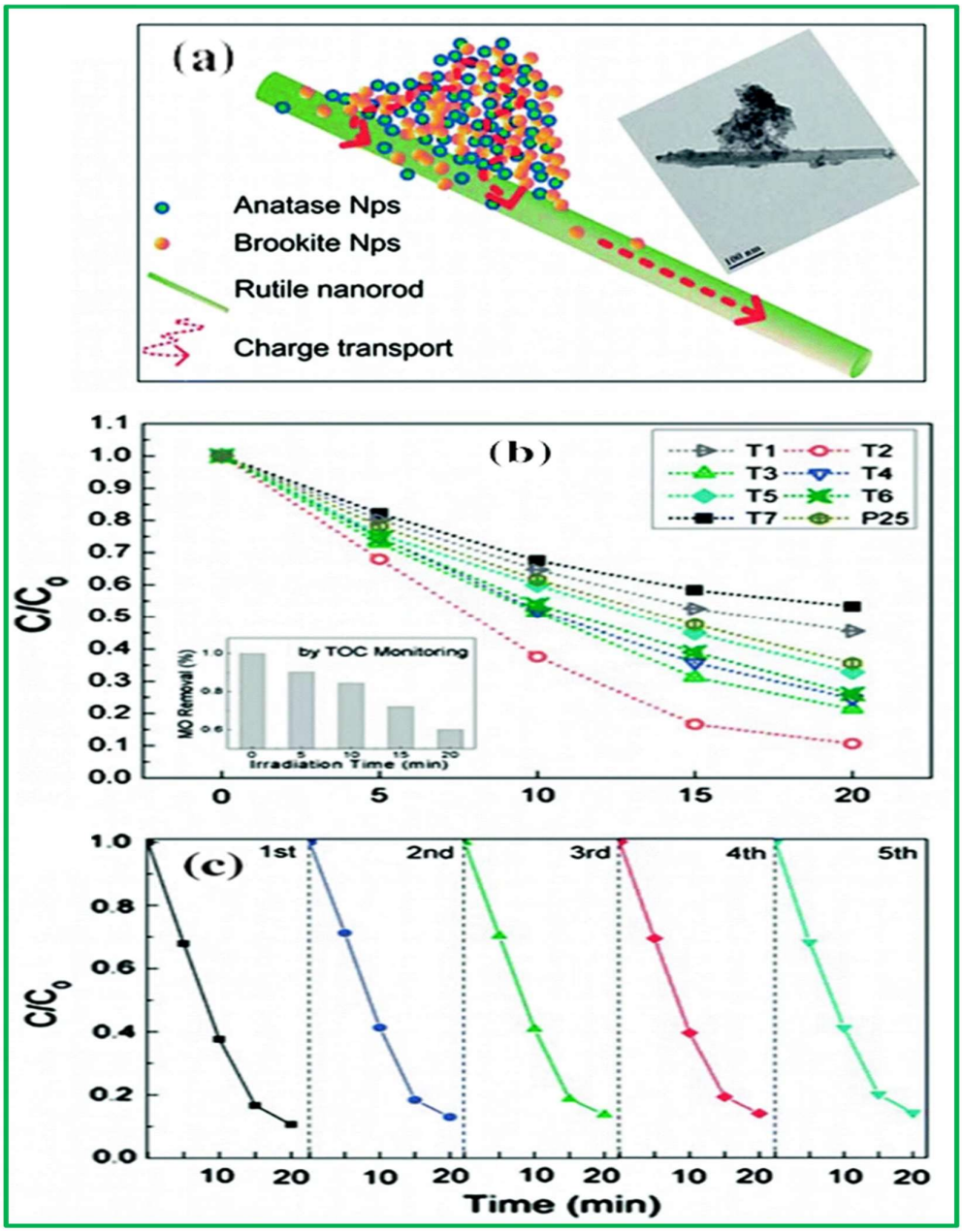

Figure 14. Schematic and SEM Image of Brookite/Anatase/Rutile Nanocomposites. A: Photocatalytic Degradation of MO Aqueous Solution Using Brookite/Anatase/Rutile Nanocomposites Synthesised Using Different Reagents, the Inset Shows MO Removal Controlled by Total Organic Carbon (TOC) with Sample T2 as Photocatalysts. B: Cyclic Degradation Curves of Coexisting Brookite/Anatase/Rutile Nanocomposites. C: For Sample T2. This Sample's Deterioration Rate Constant (k) was 0.10180min-1, Nearly Twice as High as P25's (k=0.05397min-1). Reproduced from Ref.with Permission from Royal Society.

Numerous studies have been conducted on the improved photocatalytic performance of mixed-phase TiO2 over single-phase TiO2 however, numerous issues remain. For example, distributed TiO2 nanoparticles in a mixed phase are prone to agglomeration, which significantly reduces the photocatalytic activity of materials and prevents their further growth. On the other hand, the use of mixed-phase TiO2 in photocatalysis is limited by the relatively narrow band gap of rutile, which extends the absorption of the material to part of the visible light range, but is still not sufficient to

 doi:10.20944/preprints202501.1197.v1

exploit the full spectrum of sunlight [107]. Consequently, to verify the mechanism underlying the enhanced photocatalytic activity of brookite in mixed-phase TiO2, more research is needed. Therefore, the development of mixed TiO2 nanomaterials and the integration of other useful structures (e.g., hierarchical structures), optimizing the use of visible light, and investigating the mechanism using newly developed characterization techniques will remain challenges and current research topics in this field.

The chapter summarises some effective methods and technologies for the improvement of BT-based photocatalysts for efficient CO2 reduction. It is found that the thermodynamics, kinetics and selectivity of CO2 photoreduction depend significantly on the use of visible light, the separation efficiency of photogenerated carriers and the adsorption capacity of CO2. It is shown that the configuration of surface atoms and the surface electronic structure of TiO2 brookite can be changed by adjusting the crystal facets and applying a phase shift [107]. Although the narrow band gap of rutile in the mixed phase allows the absorption of mixed-phase TiO2 to extend over part of the visible light range and provides efficient separation of photogenerated electrons and holes, thereby enhancing photocatalytic activity. It is shown that dispersed mixed-phase TiO2 nanomaterials are prone to agglomeration, which significantly reduces the photocatalytic activity.

4. MECHANISMS FOR ENHANCING THE REACTION OF CO2 REDUCTION BASED ON BT

For photocatalytic CO2 reduction, the development of highly efficient photocatalysts is usually crucial. The growth of BT is hindered by two key defects: the low utilization of visible light, limited by thermodynamic and kinetic factors, and the rapid recombination of photogenerated electrons/holes [107]. In fact, manipulation of the surface/interface of TiO2 brookite can enhance the CO2 photoreduction activity. Among them, the introduction of a co-catalyst/heterojunction structural material is crucial for carrier photogeneration, and the modification of the crystal face can enhance product selectivity and activity [108–110].

4.1. Heterojunction Construction

The theory of zone alignment states that semiconductors with distinct zone structures can form heterojunctions. An embedded electric field is created because of the different carrier concentrations on either side of the interface. This embedded electric field transfers photogenerated electrons and holes to other semiconductors, resulting in the separation of the photogenerated carriers [111]. Conventional heterojunction photocatalysts are of three different types. Semiconductors A and B in a step-gap photocatalyst (type II) have distinct zone structures, as shown in Figure 15A. The CB and VB levels of A are higher than those of B. Electron-hole pairs are spatially separated upon light irradiation, as photogenerated holes migrate to A and photoinduced electrons to B [111]. The photogeneration of electrons and holes at the anatase-brookite interface can be directly transferred due to the difference in the position of CB and VB in the TiO2 crystal phase. This facilitates the separation of the photogenerated electron-hole pairs, creating a type II heterojunction between them. As mentioned in the previous section, the creation of an anatase-BT composite was demonstrated to improve the CO2 photoreduction performance [112]. Furthermore, r-C3N4 has a small bandgap compared to that of BT. When they combine to form a hybrid, they not only enhance visible light absorption but also align well with the band position of the type-II heterojunction (Figure 15B). This helps improve the photocatalytic CO2 reduction by separating the photogenerated carriers at the interfaces [88,113].

 doi:10.20944/preprints202501.1197.v1

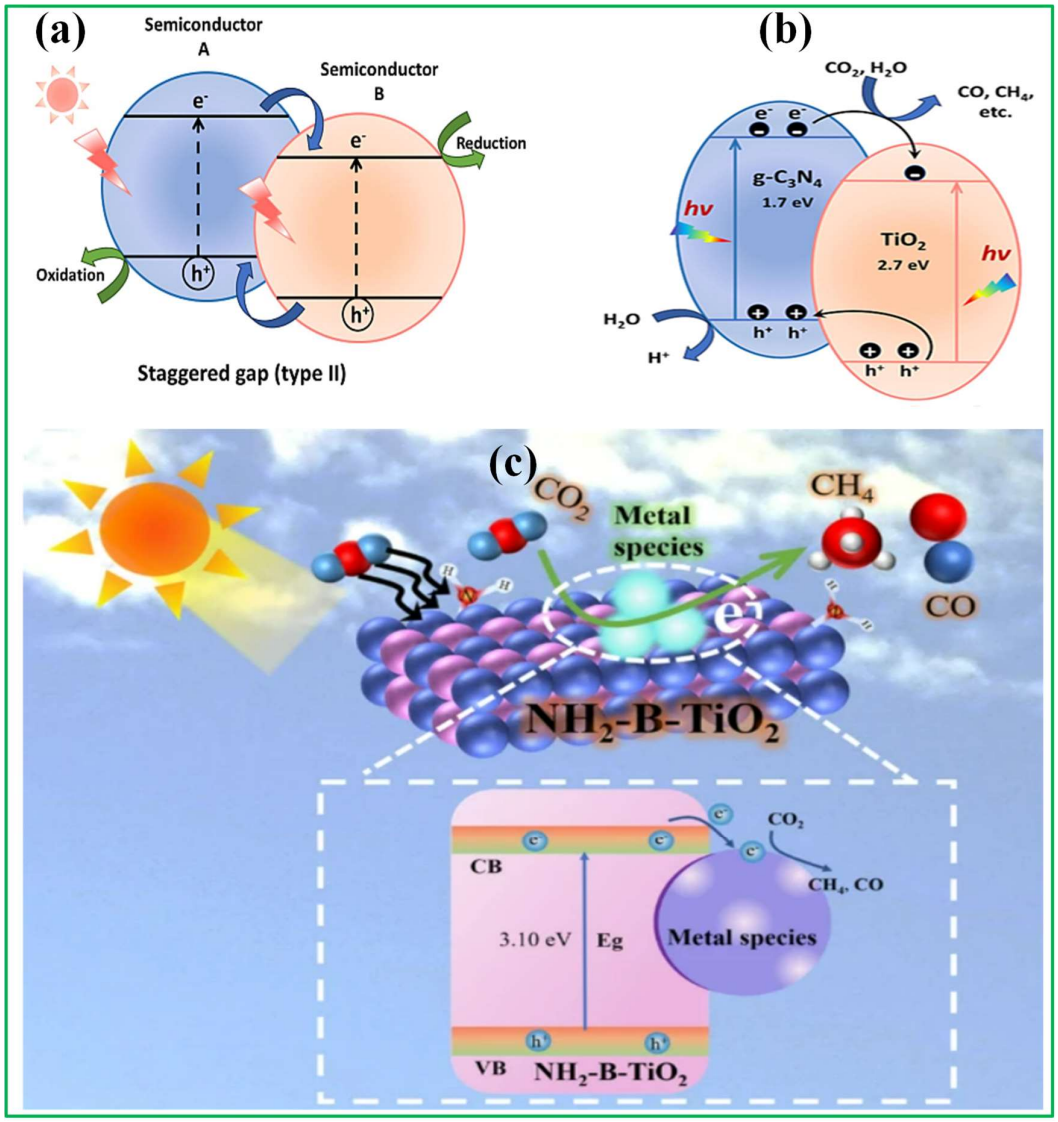

Figure 15. Illustration of the Mechanism of Charge Carriers CO2 Photoreduction on BT-photocatalysts Based on Modification Strategies. A: Type II Heterojunction; B: g-C3N4-TiO2 Heterojunction; C: Mechanism of Photocatalytic CO2 Photoreduction by BT Modified with Amine Containing Metal Particles. The figure has been significantly altered and redrawn from Ref. [90].

The physicochemical characteristics and photoactivity of titanium have been improved through the development of strategies involving heterojunction creation, heteroatom doping, oxygen vacancy creation, and cocatalyst decoration [94]. Decorating co-catalysts is one of the simplest and most effective ways to promote charge separation, enhance the adsorption-activation ability of reactants, and extend the spectral response region [114–117]. In addition, most co-catalyst loading methods are simple, which is ideal for large-scale applications and production [118–120]. To facilitate the reduction reactions in the photocatalytic CO2RR semi-catalyst, some noble metal co-catalysts (e.g., Pt, Au, and Ag) are commonly used to promote charge separation, product selectivity, and/or visible light collection (based on the localized surface plasmon resonance effect) [115–124]. However, various metal oxides, including RuOx, NiOx and MnOx, have been used as co-catalysts to regulate the photoinduced holes for the oxidative half-reaction of the photocatalytic system [125–127]. These MnOx species are of particular importance because of their non-toxicity and availability. Arash Fattah-alhosseini et al.obtained TiO2 oxide coatings incorporating ZrO2 nanoparticles formed from

 doi:10.20944/preprints202501.1197.v1

anatase and/or rutile, t-ZrO2 and ZrTiO4, which were successfully prepared on Cp-Ti using PEO process in electrolyte solutions containing zirconium nanoparticles. They showed that the higher the concentration of ZrO2 nanoparticles in the electrolyte solution, the greater the porosity, thickness and roughness of the coatings. Consequently, they are often used to harvest photoinduced holes and active sites [122–127]. Thermodynamic hole trapping is likely to be utilized to enhance the photoactivity. In addition, the joint exposure of two different types of co-catalysts to a single photocatalyst is expected to enhance the photoinduced charge separation and improve the efficiency of CO2RR [122–126]. For example, spatially separated dual CoO and Au co-catalysts can be deposited on the inner and outer surfaces of hollow TiO2 spheres as hole and electron collectors, respectively, a kind of Au@THS@CoO composite was obtained [117]. The final product provided CH4 production of 13.3μmol·g-1·h-1, which was 60 times higher than that of THS alone, and exhibited significantly enhanced activity [117]. This finding also suggests that the CO2RR efficiency is positively affected by a reasonable BT co-catalyst design.

4.2. Contribution of Doping of Metallic and Non-metallic Components

The structure and characteristics of oxide materials are known to be strongly impacted by doping with metal impurities [129]. Based on the aforementioned information, Figure 15C depicts the potential mechanism of photocatalytic CO2 reduction by metal particles acting as a co-catalyst. A certain quantity of CO2 molecules must first be adsorbed onto the surface of the photocatalyst to support the next photocatalytic CO2 reduction reaction. CO2 adsorption benefits from the use of amino functional groups as the adsorption sites. When NH2-BT is exposed to sunlight, the photogenerated holes remain in the VB, whereas the electrons in the VB are stimulated to the CB. The enhanced photocatalytic activity of CO2 photoreduction in CH4 and CO on the metal rock surface is the result of the metal particles capturing electrons after loading to provide a more effective photogenerated carrier separation. Figure 16A and 16B illustrates that following 4h of illumination, the CH4 yields of NH2-BT/Cu, NH2-BT/Ag, and NH2-BT/Ni(OH)2 are 2.37, 9.26, and 1.26μmol·g-1·h-1, respectively. These values are approximately 3.2, 12.51, and 1.7 times greater than those of pure NH2-BT (0.77μmol·g-1·h-1). In addition, following loading with metallic rocks, the trace amount of CO also improved. In NH2-BT/Cu, NH2-BT/Ag, and NH2-BT/Ni(OH)2, the CO creation rates are 2.5, 1.97, and 0.15μmol·g-1·h-1, respectively. Furthermore, NH2-BT modified with amine (0.74μmol·g-1·h-1) exhibits a greater CH4 performance than amine-free BT (0.54μmol·g-1·h-1), and metal-loaded NH2-BT composites have a CH4 performance that is almost double that of metal-loaded amine-free BT composites.

 doi:10.20944/preprints202501.1197.v1

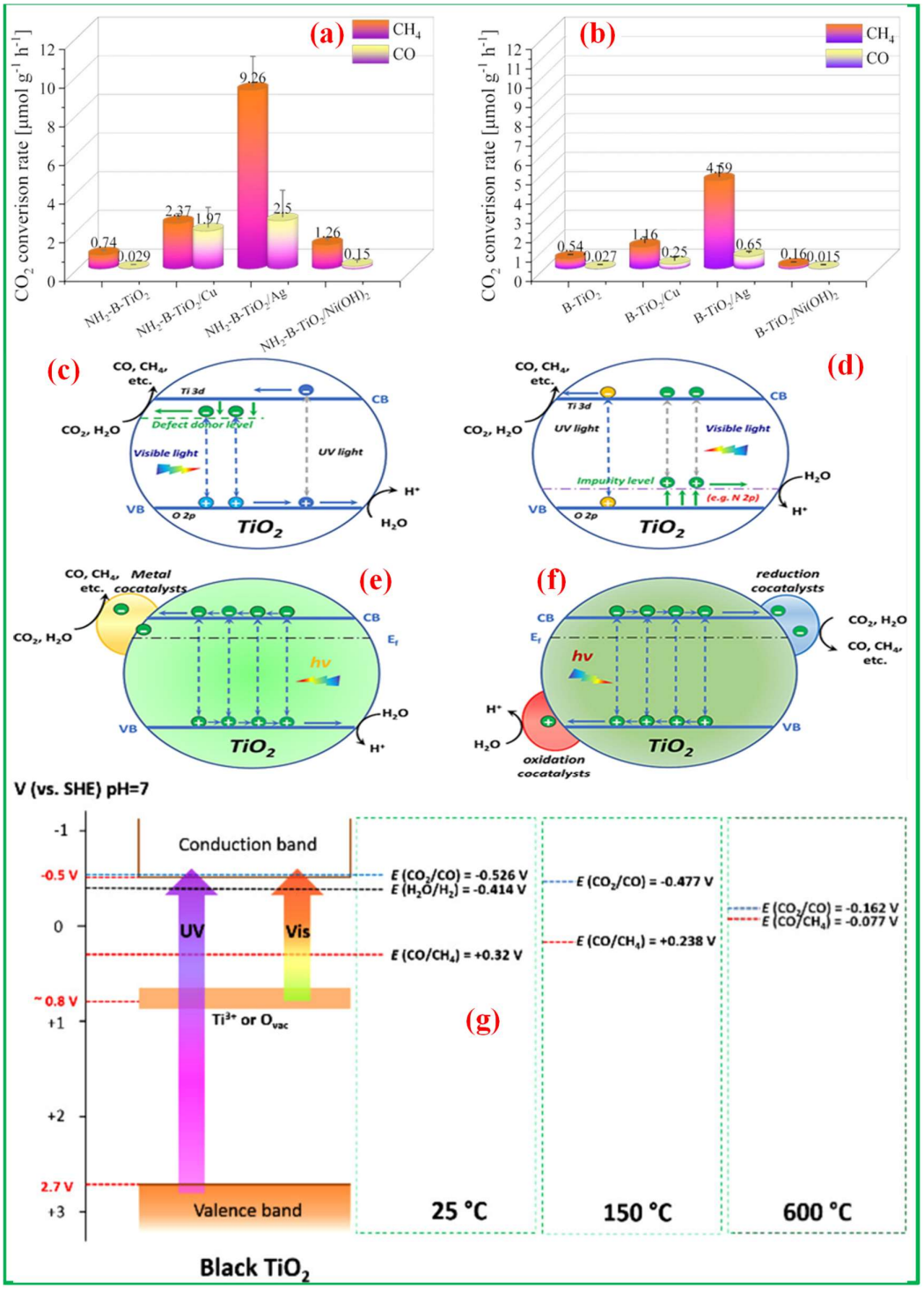

Figure 16. The ability of BT for photocatalytic reduction of CO2 taking into account the band structure and charge transfer mechanism in the presence of a cocatalyst. (A) Diagrams of Photocatalytic CO2 Reduction Activity Versus NH2-BT and its Composites and (B) Photocatalytic CO2 Reduction Activity Versus BT and its Composites; Illustration of the Charge Carrier Mechanism for CO2 Photoreduction on BT at: (C) Doping with Metal Ions, (D) Doping with Nonmetal Ions, (E) Loading of A Single Metal Co-catalyst, and (F) Loading of Dual Co-catalysts. Reproduced from Ref.with Permission from Royal Society; (G) relationship between band structure of b-TiO2 and redox potentials of CO2 reforming of CH4. Reproduced from Ref.with Permission from American Chemical Society.

 doi:10.20944/preprints202501.1197.v1

By capturing electrons in the CB, the doping of TiO2 brookite with metal ions can, on the one hand, lead to the formation of defects or change the crystallinity of the semiconductor lattice. On the other hand, doping with nonmetal ions often changes the location of the VB, and photogenerated electron-hole pairs on the TiO2 surface recombine because of competition with electrons. This extends the absorption wavelength range of TiO2 into the visible-light region and increases its photocatalytic activity. The location of the CB of TiO2 can be changed by doping with metal ions, as shown in the zone theory in Figure 16C and 16D. When properly doped with metal ions, it functioned as an interfacial medium. Dopants can achieve this goal by capturing electrons and holes and providing local separation. The trapped electrons and holes must be able to move to the reaction boundary and simultaneously be released at the same time. Doping with non-metallic elements leads to an increase in the number of oxygen vacancies on the surface and improved photocatalytic activity in visible light, in addition to improved light absorption. In 2016 Wang et. al.showed that self-doped Ti3+ hydrothermally produced BT nanosheets enhanced photocatalytic CO2 reduction activity and increased solar energy absorption. Han B et al.showed that as the temperature increased to 650°C, the reduction potential of CO2/CO became more positive and the oxidation potential of CO/CH4 became more negative. As shown in Figure 16J, one can see that those energies meet the thermodynamic requirements for visible-light photocatalytic CRM:

(I) Although CO2/CO redox potential is slightly more negative than the TiO2 CB edge at room temperature, it changes to become more positive than the CB edge at 150°C or higher. This indicates that the reduction of CO2 to CO prefers a temperature above 150°C. The redox potential of CO/CH4 is always more negative than the energy level of the Ti3+ at room temperature or above, satisfying the energy requirement for the oxidation of CH4 to CO.

(II) The energy gap (1.3eV) between the Ti3+ level and TiO2 CB ensures the absorption of visible light (and even near-infrared). This encouraged us to select the black TiO2 as a semiconductor for our catalyst. It is well-known that platinum possesses a high conductivity to transfer electrons and an excellent activity to break the C-H bonds of CH4.

4.3. Co-catalytic Effect

As mentioned above, the loading of appropriate co-catalysts can effectively enhance the photocatalytic activity of BT with respect to CO2 reduction [129,130], enhancing the photocatalytic reaction by (a) reducing the surface activation energy and loss of superpotential, (b) forming surface-active sites, and (c) forming Schottky junctions at the metal/semiconductor interface to separate the photogenerated electrons and holes [130,131].

Common metal species used to modify BT for efficient CO2 reduction in a single co-catalytic system are Ag [26], Auand Cu [85]. By interacting with these metals, such photocatalytic systems can improve the absorption of visible light and provide more active centers on the catalyst surface. A Schottky connection forms when the co-catalysts simulate contact with one another, as illustrated in Figure 16D, because they work harder than TiO2. This makes it harder for electrons stored on the metals to cross the Schottky barrier for TiO2, which prevents photoinduced electron-hole pairs from recombining [132,133]. In other words, effective photocatalytic CO2 reduction activity results from improved charge separation via the Schottky transition as well as active metal centers in the metal co-catalyst-brookite-brookite hybrid TiO2.

Reduction and oxidation co-catalysts are often present in the TiO2 brucite phase in a binary co-catalyst system. Generally speaking, transition metal oxides like CoOx, MnOx, NiO, and FeOx can act as oxidation catalysts, while metal species like Cu, Ni, Ag, Au, Pd, Pt, etc. can be utilized as reduction co-catalysts. In photocatalysis, these two types of co-catalysts work in different ways.

 doi:10.20944/preprints202501.1197.v1

Specifically, oxidizing co-catalysts are helpful for activating HO molecules and can capture holes, whereas reducing co-catalysts can improve light harvesting and electron capture. In other words, the co-utilization of these two types of co-catalysts increases the effectiveness of photocatalytic CO2 by facilitating surface catalytic processes, charge separation/transfer, and sunlight harvesting (Figure 16E). A similar occurrence was noted in a previous study [94]. Specifically, the Ag/MnOx introduction of as a dual co-catalysts may accelerate the formation of CH4, improve the adsorption and activation of CO2/H2O molecules, and encourage the separation of electron-hole pairs (Figure 16F).

4.4. Crystalline Facet Effect

One of the most researched photocatalysts is titanium dioxide (TiO2), particularly in light of its use in the photocatalytic degradation of micropollutants. During photocatalysis, TiO2 may trigger certain redox processes using photogenerated charge carriers. This process can be broken down into the following steps: (1) electrons in the TiO2 structure are excited, (2) excitons are generated and dissociate into free electrons and holes, (3) charge carriers migrate to the surface, and (4) h is transferred to the substrate that is present on the surface. Each of these phases, which is universal to all photocatalytic reactions, addresses limitations that affect the overall efficiency of the process.

Of the mentioned phenomena, steps (3) and (4) occur on the surface layers. As a result, any modification at the substrate-photocatalyst boundary can significantly change the main processes. Early photocatalytic studies that addressed topics such as surface polarization by redundant electrons, modification of precious metals, and complex surface formation by bidentate benzene derivatives to improve the transportation of charge carriers clearly indicated the importance of this boundary between the partition and the surface of the photocatalyst [134–136]. Using DFT computations and DRIFTS spectra, Liu et al.examined the adsorption of CO2 and its conversion into TiO2 crystals with various face ratios of {101}/{001}. DRIFT spectra results indicate that while a high face ratio {101}/{001} may improve the interaction between CO2 and TiO2 surfaces, it may also slow down the activation and transformation of CO2 that has been adsorbed (Figure 17A-17C). Theoretical computations have demonstrated that {001} faces lack the greater acid-alkaline features of {101} faces, which are conducive to stronger CO2 adsorption. On the other hand, CO2 binds to TiO2 if the adsorption is too intense. Thus, it is crucial to have the correct ratio of photoreduction reactions between {001} and {101} for CO.

 doi:10.20944/preprints202501.1197.v1

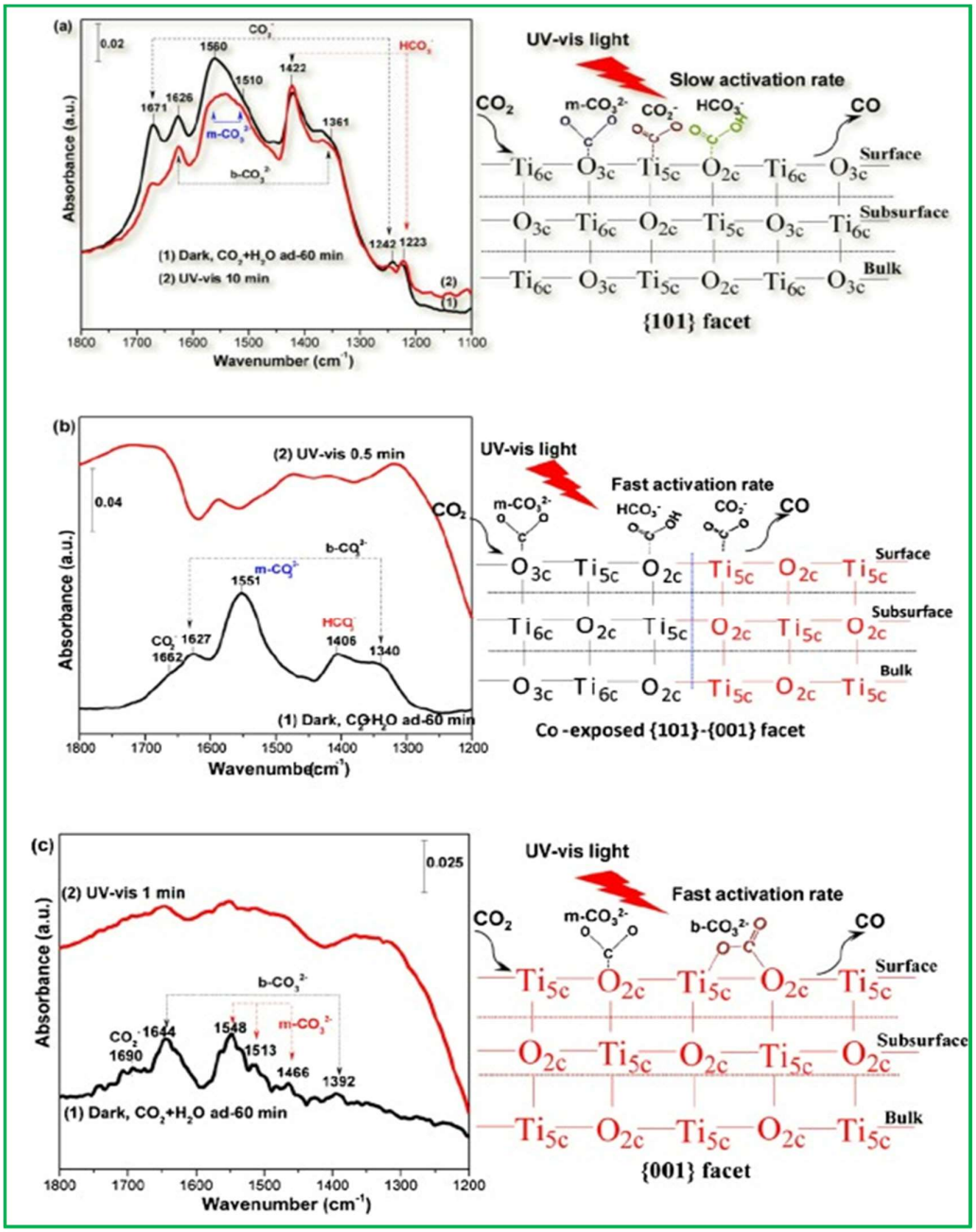

Figure 17. DRIFTS in Situ Spectra for CO2 and Water Adsorption on the BT Crystals. A: With Open {101} Faces; B: With {001}, {101}; C: {001} Faces. Reproduced from Ref.with Permission from American Chemical Society.

The development of heterojunctions other than TiO2 has also been observed in CeO2and BiOCl [139]. This suggests that one of the most frequent methods for promoting the spatial separation of photogenerated charges and enhancing the photocatalytic performance of semiconductor materials is the creation of surface heterojunctions by building open faces. As in the case of anatase and rutile TiO2, the variations in the surface energy are due to changes in the number of low-coordinated titanium atoms [140]. Using density functional theory (DTF) calculations, Zhao et al.examined the atomic structures of the {121} and {211} surfaces of BT crystals. The findings indicate that the atomic ratio of Ti4s: Ti5s: Ti6s for the {121} surface was 12.5%: 75%: 12.5%, while the atomic ratio of Ti5s: Ti6s

 doi:10.20944/preprints202501.1197.v1

for the {211} surface was 75%: 25%. The {121} surface has a greater surface energy (0.66 J/m2) than the {211} surface (0.59 J/m2) because of the presence of more uncoordinated Ti atoms (Ti4s).

The surface adsorption characteristics and surface electronic structures of the different TiO2 faces were highly variable. The redox potential of the excited charges and light absorption are determined by the electronic structure of TiO2, which also influences the photocatalytic activity. Numerous studies have reported different electron band configurations for different facets of TiO2 [142–144]. Using XPS and UV-visible absorption spectroscopy, Pan et al.verified the CB and VB potentials of the {0 1 0}, {0 0 1}, and {1 0 1} facets of anatase TiO2 crystals. According to their findings, different atomic configurations on each surface explain the larger band gaps and higher VB locations on faces {1 0 1} and {0 1 0} than on faces {0 0 1} [146]. Because the reaction at the surface is crucial for the photocatalytic process, the corresponding photocatalytic performance of the semiconductor is inextricably dependent on the atomic structure of the surface, which can be modified by crystal-phase engineering [28,146].

The surface potentials of the different crystal faces of semiconductors are different. Consequently, photoelectrons and holes can spontaneously move to different crystal faces with different energies. During catalytic processes, different crystal faces exhibit different redox properties. In addition, the ratio of the two neighboring open facets is important for the transport and separation of photogenerated carriers [147]. Ohno et al.showed that the aspect ratio during photocatalytic CO2 reduction affects the BT nanomatrices with {2 1 0} and {2 1 2} open crystal faces. Owing to electron separation, larger {2 1 0} and smaller {2 1 2} open crystal faces often avoid backlash and accelerate multielectron reduction. Ohno et al.showed that the aspect ratio during photocatalytic CO2 reduction affects the BT nanomatrices with {2 1 0} and {2 1 2} open crystal faces. Because of the separation of oxidation and reduction centers, the larger {2 1 0} and smaller {2 1 2} open crystal faces often avoid backlash and accelerate multi-electron reduction; hence, they would be the ideal surface structure for the multi-electron CO2 reduction process.

Literature analysis showed that the selectivity and activity of photocatalytic CO2 reduction correlate with the ratio of BT open faces and the co-catalyst loading. It has also been shown in many publications that doping of photocatalysts with metal or nonmetal ions improves their electronic structure and visible light absorption properties. The selectivity and activity of photocatalytic CO2 reduction correlate with the number of open facets and the co-catalyst loading. This is because the energy band structure is crucial for the photocatalytic reduction of CO2 from a thermodynamic point of view. We have considered and analysed the effects of several co-catalysts and concluded that many of them can enhance the selectivity of the reaction, act as reaction centres to reduce the overpotential of CO2 reduction and promote the separation of photogenerated electrons and holes.

5. UNRECONSTRUCTED BT SURFACES

Recently, computational techniques have been selectively used to study the precise atomic structures of potential crystal face terminations and their accompanying surface energies. This makes it possible for scientists to explain surface geometry and look into how it may alter in a new setting. Therefore, one can forecast the energy stabilization of a certain aspect to aid in its experimental acquisition. Nonetheless, the models examined are frequently investigated in vacuum, which enables researchers to assess the relative stability of various architectures and offers a helpful foundation for additional studies. However, even with many committed scholars in this field, there are still many unanswered questions that need to be thoroughly investigated. In contrast to other polymorphs, brookite surfaces frequently expose 4f-Ti and form intricate structures. The computed proportion of uncoordinated particles for brookite surfaces is only shown for Ti atoms, owing to their complexity. Furthermore, several terminations can be considered for the majority of surfaces. The models of the

 doi:10.20944/preprints202501.1197.v1

most stable brookite surfaces or those whose reconstructed geometry demonstrated notable stabilization were compiled by Szymon et al. (Figure 18) [148].

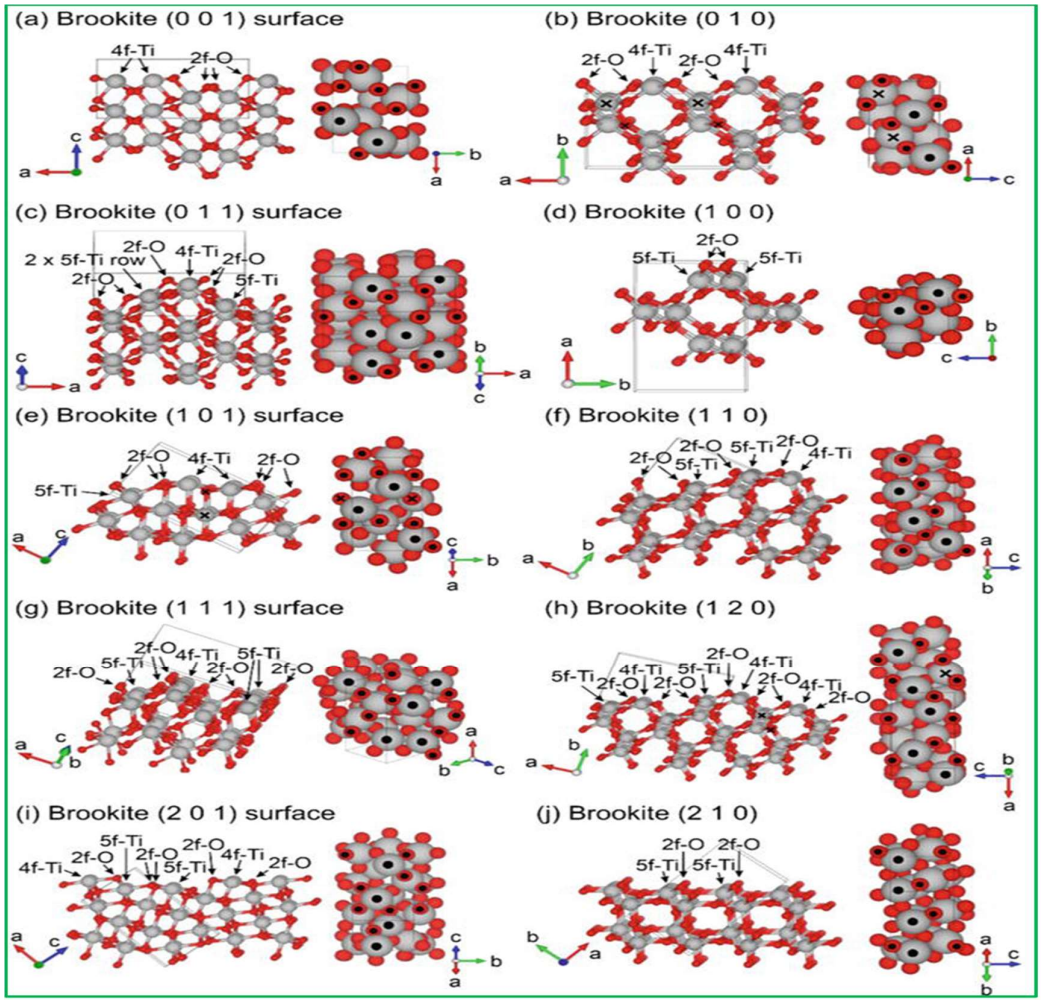

Figure 18. Perfect, bulk-cut atomic geometries of different BT surfaces. The Mark "X" Indicates Possible Bond Breaking After Relaxation [147].

The brookite surface {0 0 1} immediately exposed 4f-Ti and 6f-Ti; nevertheless, deeper areas of the surface included some additional partially exposed 6f-Ti, as Figure 18A illustrates (after incorporating a deeper Ti layer, the proportion of 4f-Ti was 1/4). The 2f-O network that links the higher Ti atoms is limited to the deeper regions of the surface where saturated O exists. Even with a basic optimization, the computed energy of this geometry was 1.18 J/m2; however, an alternative geometry may be stabilized using a potential reconstruction, which will be covered in more detail later. Furthermore, with a top layer of (2f-O)-(4f-Ti)-(2f-O) bonding to 6f-Ti in cavities, the surface structure of brookite {0 1 0} is comparable to that of anatase {1 1 0} and rutile (0 0 1). For this geometry, the proportion of 4f-Ti was 1/4, assuming exposure to the first three Ti layers. Furthermore, as indicated by a "X" in Figure 18B, relaxation reports revealed that the topmost 6f-Ti increased noticeably toward the top, breaking one link to the deeper 3f-O layer. Therefore, more 5f-Ti was expected to be exposed on the relaxed surface. This structure had a final surface energy of 0.77 J/m2. With emphasis on the above structure, the brookite surface {0 1 1} in Figure 18C exhibits a mixture of 4f-Ti (1/8), 5f-Ti (3/8), and 6f-Ti (1/2), all linked together by a complex network of both fully coordinated and uncoordinated O atoms. The uncoordinated titanium relaxes inward into the crystal

 doi:10.20944/preprints202501.1197.v1

structure, creating a final surface energy of 0.74 J/m2 , while the 6f-Ti shifts outward as a result of structure relaxation. Similar to anatase {1 1 2}, brookite {1 0 0} had a sawtooth surface profile, as shown in Figure 18D. A sequence of 5f-Ti (1/2) atoms bonded by 2f-O was visible directly at the top of the surface, whereas deeper layers showed complete coordination. As seen in Figure 18D, it should be highlighted that this structure can have two very similar but not exactly the same conFigureurations, in which the first or second Ti layer makes up the top of the surface. The surface energy of these two arrangements is somewhat different (0.88 or 0.93 J/m2) according to Gong and Selloni [149]. All things considered, their general geometry is rather similar, with the main differences between the two designs being minute differences in the precise length and angles of the connection at the top. Figure 17E illustrates the structure of an ideal {1 0 1} brookite surface, revealing the combination of 2f-coordinated O atoms with saturated and 5f-coordinated Ti (1/8) and 6f-Ti (5/8) bonds. Subsurface 6f-Ti (highlighted as «X» in Figure 18E) and a disconnect between 3f-O, which links two 4f-Ti surface atoms, are two notable alterations to the ideal structure during relaxation. The resultant 5f-Ti in this instance is in the subsurface zone, but there was also an extra 2f-O that was directly on the surface. For this shape, the resulting surface energy is 0.87 J/m2. Figure 18F shows the surface structure of brookite {1 1 0}, which is made up of terraces that terminate at the 4f-Ti edge and then continue to fall. On this surface, distinct varieties of Ti were observed. Uncoordinated atoms relax more near the margins, that is, Ti atoms relax inward and O atoms relax outward from the crystalline structure. There was 0.85 J/m2 of comparable surface energy. Gong and Selloni examined the surface of brookite {1 1 1} in detail. The most plausible {1 1 1} structure, which represents 1/8 of the Ti sites as 4-fold coordinated and 3/8 as 5f-Ti, is shown in Figure 18G. No appreciable relaxation changes were observed for this structure, and the associated surface energy was 0.72 J/m2. Figure 17H depicts the surface {1 2 0} of brookite, displaying 4f-Ti and 5f-Ti [150].

The surface model with the symbol “X” illustrates the possibility of breaking the bond between saturated Ti and O after relaxation on the additional brucite surface, resulting in the formation of a 5f-Ti site at the top of the surface. The equivalent surface energy was 0.82J/m2. In addition, no computational techniques have been used to scrutinize the brookite surface {2 0 1}; however, reports of sufficiently strong photocatalytic activity have attracted considerable experimental attention. Figure 18I shows the atomic model of the {2 0 1} surface proposed by Lin et al.atomic model of the {2 0 1} surface. Small terraces exposed to either 4f-Ti (2/7) or 5f-Ti (2/7) are scattered across this surface. In the “flat” section, two 5f-Ti atoms are connected by two 2f-O, while two 4f-Ti atoms are connected. There was an additional 2f-O at the boundary of each step. Finally, Figure 18J shows the brookite {2 1 0} surface, which is energetically the most stable, with a surface energy of 0.70J/m2. Similar steps of uncoordinated 5f-Ti bonded to 2f-O at the step edge were revealed by the atomic geometry of this surface and anatase {1 0 1}. Below the (5f-Ti)-(2f-O) steps, the lower parts of the surface were fully coordinated. For this surface, the limiting fraction of 5f-Ti was 1/2. While 5f-Ti appears to relax inward, 6f-Ti and the upper part of 3f-O relax outside the crystal structure, as in other TiO2 materials. Overall, a review of the literature shows that unlike anatase and rutile, brookite surfaces have rarely been studied. However, a comprehensive analysis of several brookite surfaces has been conducted [149], and further details regarding the {1 0 1}, {1 2 1}, and {2 0 1} structures are available [150].

Key points of the chapter. It has been reported in the literature that brookite surfaces form rather complex structures, often exposing 4f-Ti. Due to this complexity, the calculated fraction of undercoordinated species for brookite surfaces is presented only for Ti atoms. Moreover, in the case of most surfaces, multiple endings can be considered.

6. ADVANTAGES OF BROOKITE PHOTOCATALYSIS IN RELATION TO ANATASE AND RUTILE

 doi:10.20944/preprints202501.1197.v1

Anatase, brookite and rutile were used in the study by Zhang et al.to study the photocatalytic degradation of rhodamine B. The authors showed that the degradation efficiency of rhodamine B increased with the order of anatase, rutile and brookite. It was also observed that for the degradation and mineralization of various pharmaceutical chemicals and phenol, brookite was a better photocatalyst than anatase and rutile [153]. When the degradation of tetramethylammonium and 4-chlorophenol was compared, the photocatalytic activities of anatase, brookite and rutile were also investigated [154]. When it came to tetramethylammonium and 4-chlorophenol, brookite had the highest photodegradation efficiency. The application of different TiO2 polymorphs for photocatalytic hydrogen production resulted in a hydrogen production rate of 0.9742μmol·h-1·m-2 from brookite and 0.3719μmol·h-1m-2 from anatase [154]. The main discrepancy is that the rate of hydrogen synthesis by photoreforming is about 5 times higher than conventional water splitting, even though the high hydrogen production using brookite is consistent with the results of this study (Figure 19A and 19B). This suggests that photoreforming not only increases hydrogen production activity, but also breaks down plastic waste and avoids costly sacrificial electron donors such as methanol in water splitting.

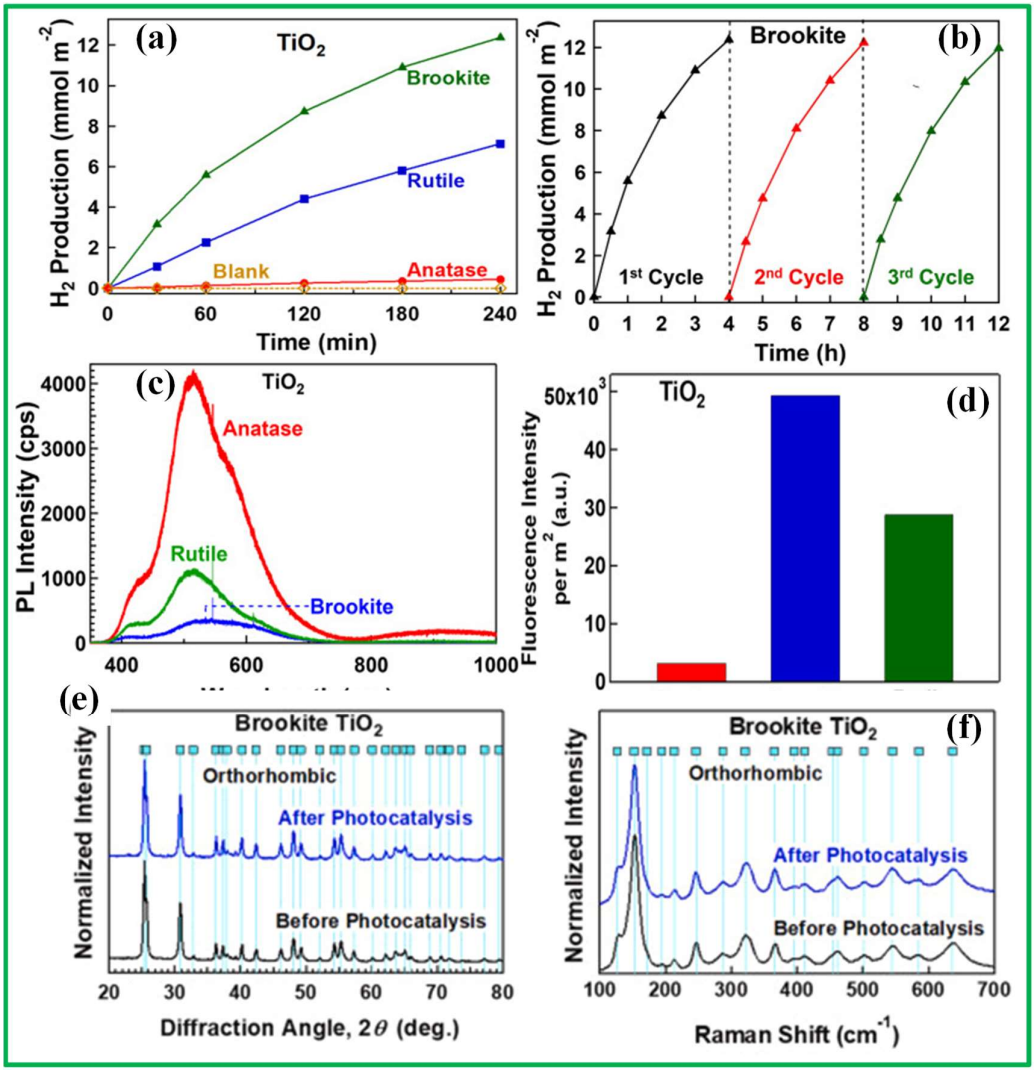

Figure 19. Photocatalytic Hydrogen Production From PET Plastic Degradation Using Anatase, Brookite and Rutile. A: Including Blank Data; B: Recyclability of Brookite TiO2 Catalyst; C: PL Spectrum of Anatase, Brookite and Rutile at 325nm; D: Fluorescence Intensity of TiO2 at 450nm after 20min Irradiation; E: X-ray Diffraction; F:

 doi:10.20944/preprints202501.1197.v1

Raman. Spectra of BT Before and After the Photocatalytic Reaction. Reproduced from Ref.with Permission from Elsevier.

The study demonstrates that the recombination rate of charge carriers during photocatalytic reduction of CO2 is one of the primary determinants in the adoption of brookite over other phases [156]. The photoluminescence signals, which indicate the degree of radiative recombination of photogenerated electrons and holes, rise with the order of brookite, rutile, and anatase, as Figure 18C and 18D illustrated. As a result, of photogenerated electron-hole pairs, brookite has the lowest radiative recombination. According to Choi et al.'s investigation on the charge transfer kinetics of brookite and anatase, brookite has a charge transfer resistance that is significantly lower than anatase's, making it easier to separate the charge carriers in brookite [154]. Anatase and brookite have significantly lower conductivity when it comes to the rapid transfer of photogenerated electrons, according to studies using open circuit voltage decay [157]. In addition, it has been shown using time-resolved photoluminescence spectroscopy that brookite decays slower than anatase. According to this, the charge carriers in brookite have a longer lifetime and a lower recombination rate, leading to the formation of ·OH and hydrogen radicals, which are also shown in current photoreformation studies [157]. Regarding the stability issues of brookite-based photocatalysts, despite previous claims, Thanh Tam Nguyen and Kaveh Edalatishowed that BT retains its suitability for reuse very well (Figure 19E, 19F and 19B). In this study, the authors showed that there is no noticeable change in the Raman spectra as well as the X-ray diffraction pattern, which speaks about the stability of BT for the photocatalytic process. The depth of charge carrier traps, as previously shown, can both increase and decrease the lifetime of electrons, which explains why anatase, brookite, and rutile exhibit different levels of photocatalytic activity [158]. When electrons and holes have long lifetimes, a reasonable depth of traps can ensure that they remain reactive, aiding in reduction and oxidation processes. The number and lifetime of holes in brookite have been found to increase when there are somewhat deep electron traps in the mid-shell states [159]. Electron traps in brookite are deeper than in anatase and shallower than in rutile, according to the results of a study of the behavior of photogenerated electrons and holes in TiO2, in which absorption spectroscopy in the visible and mid-infrared regions was used [160]. According to the results, the depth of electron traps for rutile, brookite and anatase were 0.9, 0.4 and 0.1eV, respectively [160]. It turned out that most of the photogenerated electrons in brookite are trapped by defects within picoseconds, which has a double effect - a decrease in the number of free electrons and a lengthening of the electron lifetime. The high activity of brookite in the photoreformation of CO2 and plastic waste is also explained by the fact that the large number of holes is a favorable characteristic for accelerating photocatalytic oxidation processes. Compared to rutile and anatase, brookite shows higher photocatalytic activity. This can be explained by a number of factors such as strong ·OH radical formation, moderate carrier trapping depth, long degradation process and efficient charge separation. The low activity of anatase practically ruled out the use of TiO2 for photoreforming; however, the present results open the possibility for the use of brookite TiO2. Other advantages of using brookite include its excellent environmental qualities. Considering the strong correlation between crystal structure and photoreforming activity, other TiO2 polymorphs for photoreforming are worth investigating in the future. Examples include the high-pressure columbite phase, which shows high CO2 conversion activity [161], and mixtures of different TiO2 phases, such as the P25 catalyst [162,163].

The crystal structure and band structure of semiconductor photocatalysts greatly affect their light absorption ability. Three polymorphs of TiO2 have been extensively studied in the past few years and have achieved significant progress in the photocatalytic reduction of CO2 [164]. In the ultraviolet light range, the light absorption ability of TiO2 has been shown to be limited for anatase and rutile, and only brookite is the best due to its favorable structural modification. However, extensive research is still required for brookite to achieve the desired level of photocatalytic activity.

 doi:10.20944/preprints202501.1197.v1

A dopant-free method to enhance the light absorption in pure TiO2 crystal has also been recently investigated [165]. The band gap of TiO2 has been shown to decrease under high pressure theoretically [166]. For example, the band gap of nanoscale TiO2-II (columbite) phase was reported by Hadi Razavi-Khosroshahi et al.to be approximately 2.4eV. The TiO2-II polymorph prepared by high-pressure torsion processing was found by Wang et al.to have excellent visible light photocurrent performance. For photocatalytic CO2 reduction, it can be concluded that the development of TiO2 polymorphs to enhance the light absorption ability of titanium dioxide is an effective modification strategy.

In the present section, the photocatalytic activity of TiO2 polymorphs anatase, brookite and rutile has been discussed and compared. It was found that the yield of degradation products depends on the phase of TiO2. The photocatalytic activity was found to increase in the order of anatase, rutile and brookite. The photocatalytic activity of brookite for photocatalytic CO2 reduction has been investigated by various scientists, although the number of relevant publications is small, so it is necessary to go deeper into the study and photocatalytic application of brookite for other CO2 photoreduction reactions and photoreforming of plastic waste, and to carry out careful DFT calculations to find out the high photocatalytic activity of brookite with regard to charge carrier separation, transport, recombination and trap depth.

7. OPPORTUNITIES AND APPLICATIONS

Despite many years of research, BT remains a highly sought-after material owing to its exceptional photocatalytic activity. The use of BT is expected to attract much attention as more serious energy and environmental problems emerge. Necessary steps are being taken, and new mechanisms are being developed to improve the photocatalytic CO2 reduction reaction involving brookite [169–172]. Despite the possibility of combining several modification methods to create highly efficient hybrid photocatalysts, the mechanisms by which the different components work together. In particular, to directly measure the kinetics of the charge transfer channel and active center, a better characterization approach is required [172]. To comprehensively understand the correlation between the CO2 activity/selectivity of photoreduction and the movement of active centers/charges, knowledge of the catalytic process at the electronic and molecular levels should be connected to both in situ approaches and theoretical calculations. Because thin-layer photocatalysts have special features, they can be used to reduce photoreductive effects in structural design. Usually, only a few or even one atom forms the thickness of an ultrathin 2D material. Because of its high surface area, it can absorb UV and visible light more effectively than other materials because it has more reactive active centers and low-coordinated atoms. Simultaneously, actual surface-active objects are impacted by thin-layer 2D materials, which tend to form dense stacking structures [173]. In this case, the electrical structure of the thin-layer structure can be corrected, and additional active centers can be revealed by the participation of several mesopores. Furthermore, by adding oxygen vacancies to the BT thin layer using a variety of techniques, such as thermal, solvothermal, reduction, and photochemical treatments, it is possible to improve light harvesting while simultaneously providing a channel for charge transfer to the CO2 photoreduction, adsorption, and activation sites.

Doping BT with nonmetallic heteroatoms to modify its local electronic structure and improve light utilization and charge separation is a viable strategy. Specifically, the introduction of heteroatoms into a pristine lattice may impure the development levels [174]. This effect accelerates the separation of electron-hole pairs and extends the light adsorption range. Furthermore, the CO2 adsorption state is affected because the inclusion of heteroatoms increases the local electron density. Crucially, a great deal of work will be done using theoretical calculations and modeling to fully comprehend the function of doping sites in CO2 adsorption kinetics and reactions. In general, the effectiveness of BT modified with a single co-catalyst for CO2 photoreduction is limited. On the one

 doi:10.20944/preprints202501.1197.v1

hand, research into novel co-catalysts for BT-based CO2 reduction that exhibit high activity, selectivity, stability, and low cost is crucial. Another tactic is the logical design of a single-atom-embedded BT Photocatalysis System. Single-atom catalysts exhibit high activity, maximal atom utilization, and high selectivity and are therefore often used in catalysis applications. According to a previous study, when used in conjunction with two co-catalysts, BT may provide a variety of sites and channels for charge migration and separation as well as catalytic CO2 reduction and H2O oxidation during photocatalytic CO2 conversion [175,176].

Binary co-catalysts, including metals, hydroxides, phosphides, and carbon-containing materials, can be used as reduction co-catalysts to capture electrons in similar systems. Dual reduction/oxidation co-catalysts can be simultaneously added to BT oxidation. In general, the recombination of photoinduced charge carriers can be suppressed by creating transition-metal oxides such as MnO. The localized effect of surface plasmon resonance can also lead to increased light absorption in certain plasmonic noble metals. Therefore, the kinetics of surface reactions can be enhanced by a binary reductive co-catalyst containing noble metals, and it is important to consider how the composition of dual-metal co-catalysts affects the production selectivity. In particular, the adsorption capacity for CO photoreduction varies among metallic steels with different exposed faces [177]. Additionally, various binary metal co-catalysts (such as alloys, intermetallides, and two independent metal nanoparticles) can be used to adapt their intrinsic electronic properties to engineer the activity and selectivity in CO for electron/hole trapping and photocatalytic CO2 reduction. NiO, CoOx, and RuO2 can also be used as oxidation co-catalysts. However, there is an urgent need to address the problem of controlling remote dual co-catalysts with different functionalities. An effective method for creating active centers and catalyzing the photocatalytic process is the creation of cocatalysts for metal reduction in BT. Another significant difficulty is differentiating the selectivity of CO2 photoreduction owing to the action of metal/metal and BT molecules and intermediates [178]. However, there is an urgent need to address the problem of controlling remote dual co-catalysts with different functionalities.

Because reduction and oxidation reactions occur on BT, which has a lower reduction potential, and on p-type semiconductors, which have a lower oxidation potential, an analysis of the literature has demonstrated that the formation of heterojunctions in TiO2 reduces the redox capabilities of the p-n junction. The aforementioned issue was avoided by a recently developed step-scheme heterojunction (S-scheme) [179,180].. Reductive photocatalysts and oxidation photocatalysts with well-matched band structures often exhibit S-scheme transitions. Photogenerated electrons and holes are collected on the valence and CBs, respectively, during this transition. In this sense, the CO2 photoreduction process benefits from the ability of the photocatalytic system to stop charge-carrier recombination and maintain a high redox potential.

The effective CO2 photoreduction of future tailored BT systems can be attributed to the movement and spatial separation of the photogenerated charge carriers. In general, three different types of compounds, crystalline facet transition, homophase, and heterophase BT, can be used as photocatalytic CO2 reduction agents. Because TiO2 is a typical n-type semiconductor, it can be bonded to a p-type semiconductor (Cu2O, CuO, Ag2O, etc.), and the resulting p-n heterojunction can efficiently separate photoinduced electrons and holes through an internal electric field. While co-exposed BT faces with distinct morphologies or exposed crystal faces can have varied band-energy structures and band-edge locations, BT can create a homojunction between them by varying the reaction conditions) [181–192]. Consequently, a surface heterojunction formed inside the morphological BT can facilitate the separation and transport of interfacial electrons and holes.

 doi:10.20944/preprints202501.1197.v1

8. CONCLUSION

A review of the literature shows that, despite the best efforts of researchers, the most underestimated difficulty in TiO2-based photocatalytic techniques is the optimization of bare BT. Three main problems can be distinguished: First, obtaining a pure brookite phase is a problem. Second, pure BT is not photocatalytically active in the absence of co-catalysts or structural modifications of the dopant. Ultimately, because BT is metastable and converts to rutile at high temperatures, it is difficult to obtain a pure BN phase as opposed to a mixture containing TiO2 anatase. In general, it is possible to vary the hydrothermal reaction temperature, electrolyte concentration, pH, reaction duration, sample size, and crystalline phase by using various additives. Several surfactants, including PVP, PVA, and NaBH2, were reviewed. The shape and reaction process of BT can be controlled using hydrothermal technology, which is considered one of the easiest ways to produce BT. There are several methods for improving the efficiency of TiO2 brookite-based photocatalysts for CO2 reduction. The thermodynamics, kinetics, and selectivity of CO2 photoreduction depend significantly on the utilization of visible light, the separation efficiency of the photogenerated carriers, and the adsorption capacity of CO2. The configuration of surface atoms and electronic structure of TiO2 brookite can be modified by adjusting the crystal faces and applying a phase shift. Despite the fact that the narrow band gap of rutile in the mixed phase allows extending the absorption of mixed-phase TiO2 to a part of the visible-light range and provides effective separation of photogenerated electrons and holes, thus increasing the photocatalytic activity, it has been shown that dispersed TiO2 nanomaterials with mixed phases are prone to agglomeration, which significantly reduces their photocatalytic activity.

The interfacial electron transfer kinetics and photovoltaic conversion characteristics were found to depend significantly on the crystalline facets of BT, and the photocatalytic processes of CO2 and H2O adsorption states were investigated. In addition, the selectivity and activity of the photocatalytic CO2 reduction were correlated with the ratio of BT open faces to co-catalyst loading. A literature study showed that doping photocatalysts with metal or nonmetal ions improves their electronic structure and visible-light absorption properties. The selectivity and activity of the photocatalytic CO2 reduction were correlated with the number of open facets and the co-catalyst loading. This is because the energy band structure is crucial for the photocatalytic reduction of CO2 from a thermodynamic perspective. We considered and analyzed several co-catalysts that can enhance the selectivity of the reaction, act as reaction centers to reduce the overpotential of CO2 reduction, and promote the separation of photogenerated electrons and holes. An efficient photocatalytic system with a wide range of light absorption, high charge separation efficiency, and multiple active centers should be developed as a result of the growing interest in crystal facet control, heteroatom doping, phase transition creation, and heterojunctions in BT-mediated CO2 photoreduction.

Acknowledgements

The work was performed at the S.U. Umarov Physical-Technical Institute of the National Academy of Sciences of Tajikistan with the support of International Science and Technology Center (ISTC), project TJ-2726. The author expresses his deep gratitude to the Government of Japan for financial support of this project and the establishment of a modern laboratory at the PhTI, NAST.

Conflicts of Interest

The author declared no conflict of interest.

Author Contribution

 doi:10.20944/preprints202501.1197.v1

The sole author, Dr. Dilshod Nematov, confirms responsibility for all aspects of the study. This includes conceptualization, data collection, literature review and interpretation of results, writing of the manuscript and final approval of the version to be published.

Abbreviation List

AQY, Apparent quantum yield
BT, Brookite titanium dioxide
CB, Conduction band
VB, Valence band
CO2RR, CO2 reduction reaction
DFT, Density functional theory
MO, Methyl orange
PVA, Polyvinyl alcohol
PVP, Polyvinylpyrrolidone
XPS, X-ray photoelectron spectroscopy

References

1. Lai W, Qiao Y, Zhang J et al. Design strategies for markedly enhancing energy efficiency in the electrocatalytic CO2 reduction reaction. *Energ Environ Sci*, 2022; 15: 3603-3629. [DOI]
2. Brausmann A, Bretschger L. Escaping Damocles' Sword: Endogenous Climate Shocks in a Growing Economy. *Environ Resour Econ*, 2024; 87: 1545-159. [DOI]
3. He Y, Lei Q, Li C et al. Defect engineering of photocatalysts for solar-driven conversion of CO2 into valuable fuels. *Mater Today*, 2021; 50: 358-384. [DOI]
4. Schuurmans JH, Masson TM, Zondag SD et al. Solar-Driven Continuous CO2 Reduction to CO and CH4 using Heterogeneous Photothermal Catalysts: Recent Progress and Remaining Challenges. *ChemSusChem*, 2024; 17: e202301405. [DOI]
5. Yan K, Chen L, Hu Y et al. Accelerating solar driven CO2 reduction via sulfur-doping boosted water dissociation and proton transfer. *Nano Res*, 2024; 17: 1056-1065. [DOI]
6. Creissen CE, Fontecave M. Solar-Driven Electrochemical CO2 Reduction with Heterogeneous Catalysts. *Adv Energy Mater*, 2021; 11: 2002652. [DOI]
7. Chang X, Wang T, Gong J. CO2 photo-reduction: insights into CO2 activation and reaction on surfaces of photocatalysts. *Energ Environ Sci*, 2016; 9: 2177-2196. [DOI]
8. Yang J, Wang D, Han H et al. Roles of cocatalysts in photocatalysis and photoelectrocatalysis. *Accounts Chem Res*, 2013; 46: 1900-1909. [DOI]
9. Ran J, Jaroniec M, Qiao SZ. Cocatalysts in semiconductor-based photocatalytic CO2 reduction: Achievements, challenges, and opportunities. *Adv Mater*, 2018; 30: 1704649. [DOI]
10. Chang X, Wang T, Yang P et al. The development of cocatalysts for photoelectrochemical CO2 reduction. *Adv Mater*, 2019; 31: 1804710. [DOI]
11. Ovenstone J, Chan KC. Effect of halide contaminant ions in the hydrothermal treatment of amorphous titania on the phase change from anatase to rutile during calcination. *Eur J Inorg Chem*, 2001; 2001: 1339-1342. [DOI]
12. Kapsalis V, Kyriakopoulos G, Zamparas M et al. Investigation of the photon to charge conversion and its implication on photovoltaic cell efficient operation. *Energies*, 2021; 14: 3022. [DOI]
13. Dambournet D, Belharouak I, Amine K. Tailored preparation methods of TiO2 anatase, rutile, brookite: mechanism of formation and electrochemical properties. *Chem Mater*, 2010; 22: 1173-1179. [DOI]
14. Eddy DR, Sheha GAN, Permana MD. Study on triphase of polymorphs TiO2 (anatase/rutile/brookite) for boosting photocatalytic activity of metformin degradation. *Chemosphere*, 2024; 35: 141206. [DOI]
15. Simons PY, Dachille F. The structure of TiO2 II, a high-pressure phase of TiO2. *Acta Crystallogr*, 1967; 23: 334-336. [DOI]
16. Latroche M, Brohan L, Marchand R. New hollandite oxides: TiO2(H) and K0.06TiO2. *J Solid State Chem*, 1989; 81: 78-82. [DOI]
17. Cromer DT, Herrington K. The structures of anatase and rutile. *J Am Chem Soc*, 1955; 77: 4708-4709. [DOI]
18. Choi M, Lim J, Baek M. Investigating the unrevealed photocatalytic activity and stability of nanostructured BT film as an environmental photocatalyst. *Acs Appl Mater Inter*, 2017; 9: 16252-16260. [DOI]
19. Di Paola A, Bellardita M, Palmisano L. Brookite, the Least Known TiO2 Photocatalyst. *Catalysts*, 2013; 3: 36-73. [DOI]
20. Xiong J, Zhang M, Cheng G. Facile polyol-triggered anatase–rutile heterophase TiO2-x nanoparticles for enhancing photocatalytic CO2 reduction. *J Colloid Interf Sci*, 2020; 579: 872-877. [DOI]

21. Mo S, Ching W. Electronic and optical properties of three phases of titanium dioxide: Rutile, anatase and brookite. *Phys Rev B*, 1995; 51: 13023-13032. [DOI]
22. Manzoli M, Freyria FS, Blangetti N et al. Brookite, a sometimes under evaluated TiO2 polymorph. *Rsc Adv*, 2022; 12: 3322-3334. [DOI]
23. Zhao W, Li Y, Shen W. Tuning the shape and crystal phase of TiO2 nanoparticles for catalysis. *Chem Commun*, 2021; 57: 6838-6850. [DOI]
24. Ye Z, Ye Z, Nikiforov A et al. Influence of mixed-phase TiO2 on the activity of adsorption-plasma photocatalysis for total oxidation of toluene. *Chem Eng J*, 2021; 407: 126280. [DOI]
25. Billo T, Fu FY, Raghunath P et al. Ni-nanocluster modified black TiO2 with dual active sites for selective photocatalytic CO2 reduction. *Small*, 2018; 14: 1702928. [DOI]
26. Li K, Peng T, Ying Z et al. Ag-loading on BT quasi nanocubes with exposed {2 1 0} and {0 0 1} facets: Activity and selectivity of CO2 photoreduction to CO/CH4. *Appl Catal B-Environ*, 2016; 180: 130-138. [DOI]
27. Zhang W, He H, Li H et al. Visible-light responsive TiO2-based materials for efficient solar energy utilization. *Adv Energy Mater*, 2021; 11: 2003303. [DOI]
28. Xiong Z, Lei Z, Li Y et al. A review on modification of facet-engineered TiO2 for photocatalytic CO2 reduction. *J Photoch Photobio C*, 2018; 36: 24-47. [DOI]
29. Saberyoun A, Fattah-alhosseini A, Karbasi M et al. Boosting the Visible-Light-Driven Photocatalytic Efficiency in Porous Cu/TiO2 Ceramic Coatings. *Ceram Int*, 2024; 50: 31313-31325. [DOI]
30. Li Y, Wei Y, He W et al. Ordered macroporous structured TiO2-based photocatalysts for CO2 reduction: A review. *Chin Chem Lett*, 2023; 108417. [DOI]
31. Ohtani B, Handa JI, Nishimoto SI et al. Highly active semiconductor photocatalyst: Extra-fine crystallite of BT for redox reaction in aqueous propan-2-ol and/or silver sulfate solution. *Chem Phys Lett*, 1985; 120: 292-294. [DOI]
32. Yang J, Wang J, Wang G, et al. In situ irradiated XPS investigation on S-scheme TiO2/Bi2S3 photocatalyst with high interfacial charge separation for highly efficient photothermal catalytic CO2 reduction. Journal of Materials Science & Technology, 2024; 189: 86-95. [DOI]
33. Feng K, Sun T, Hu X, et al. 0D/2D Co 0.85 Se/TiO2 p–n heterojunction for enhanced photocatalytic H2 evolution. Catalysis Science & Technology, 2022; 12(15): 4893-4902.
34. Dambournet D, Belharouak I, Amine K. Tailored preparation methods of TiO2 anatase, rutile, brookite: mechanism of formation and electrochemical properties. *Chem Mater*, 2010; 22: 1173-1179. [DOI]
35. Ullattil SG, Periyat P. Sol-gel synthesis of titanium dioxide. *Sol-gel Mater Energ Environ Electron Appl*, 2017; 2017: 271-283. [DOI]
36. Koelsch M, Cassaignon S, Guillemoles JF et al. Comparison of optical and electrochemical properties of anatase and BT synthesized by the sol-gel method. *Thin Solid Films*, 2002; 403: 312-319. [DOI]
37. Nachit W, Ahsaine HA, Ramzi Z et al. Photocatalytic activity of anatase-BT nanoparticles synthesized by sol gel method at low temperature. *Opt Mater*, 2022; 129: 112256. [DOI]
38. Johari ND, Rosli ZM, Juoi JM et al. Heat treatment temperature influence on the structural and optical properties of BT thin film synthesized using green sol-gel route. *J Adv Manuf Tech*, 2021; 15.
39. Ioannidou T, Anagnostopoulou M, Vasiliadou IA et al. Mixed phase anatase nanosheets/brookite nanorods TiO2 photocatalysts for enhanced gas phase CO2 photoreduction and H2 production. *J Environ Chem Eng*, 2024; 12: 111644. [DOI]
40. Vajedi FS, Dehghani H. Synthesis of titanium dioxide nanostructures by solvothermal method and their application in preparation of nanocomposite based on graphene. *J Mater Sci*, 2016; 51: 1845-1854. [DOI]
41. Prado LR, Figureueiredo RT, Silva RS et al. Reactive precipitation of titanium dioxide particles in supercritical CO2 by SAS technique with an ionic liquid as adjuvant. *Braz J Chem Eng*, 2024; 41: 287-298. [DOI]
42. Wu Z, Wang L, Wang Y et al. A novel hydrothermal method to synthesize brookite titanium dioxide nanosquares for efficient pollutant degradation. *Environ Chem Lett*, 2023; 21: 3071-3076. [DOI]
43. Szołdra P, Frąc M, Lach R et al. Effect of brookite on the photocatalytic properties of mixed-phase TiO2 obtained at a higher temperature. *Mater Sci Eng B*, 2023; 287: 116104. [DOI]
44. Díaz-Real JA, Ma J, Alonso-Vante N. Highly photoactive Brookite and Anatase with enhanced photocatalytic activity for the degradation of indigo carmine application. *Appl Catal B-Environ*, 2016; 198: 471-479. [DOI]
45. Zhang Z, Wu Q, Johnson G et al. Generalized synthetic strategy for transition-metal-doped brookite-phase TiO2 nanorods. *J Am Chem Soc*, 2019; 141: 16548-16552. [DOI]
46. Zhang Q, Li C. High temperature stable anatase phase titanium dioxide films synthesized by mist chemical vapor deposition. *Nanomaterials*, 2020; 10: 911. [DOI]
47. Alotaibi AM, Sathasivam S, Williamson BA. Chemical vapor deposition of photocatalytically active pure BT thin films. *Chem Mater*, 2018; 30: 1353-1361. [DOI]
48. Bozok SS. Embedding anatase, rutile, and brookite TiO2 nanoparticles to cotton fabric with epoxy silane and comparison of their effects on photodegradation. *Pigm Resin Technol*, 2024; ahead-of-print. [DOI]

49. Ohno T, Higo T, Saito H et al. Dependence of photocatalytic activity on aspect ratio of a BT nanorod and drastic improvement in visible light responsibility of a BT nanorod by site-selective modification of Fe3+ on exposed faces. *J Mol Catal A-Chem*, 2015; 396: 261-267. [DOI]
50. Lu H, Zhong J, Ji C, et al. Fabricating an optimal rutile TiO2 electron transport layer by delicately tuning TiCl4 precursor solution for high performance perovskite solar cells. *Nano Energy*, 2020; 68: 104336. [DOI]
51. Nematov D. Bandgap tuning and analysis of the electronic structure of the Cu2NiXS4 (X= Sn, Ge, Si) system: mBJ accuracy with DFT expense. *Chem. Inorg. Mat*, 1, 100001. [DOI]
52. Wang J, Sun J, Bian X. Preparation of oriented TiO2 nanobelts by microemulsion technique. *Mater Sci Eng A*, 2004; 379: 7-10. [DOI]
53. Truong QD, Le TH, Hoa HT. Amino acid-assisted controlling the shapes of rutile, brookite for enhanced photocatalytic CO2 reduction. *CrystEngComm*, 2017; 19: 4519-4527. [DOI]
54. Zou Y, Tan X, Yu T et al. Controllable preparation of flower-like BT nanostructures via one-step hydrothermal method. *Mater Res Bull*, 2016; 80: 237-242. [DOI]
55. Yang Z, Wang B, Cui H et al. Synthesis of crystal-controlled TiO2 nanorods by a hydrothermal method: rutile and brookite as highly active photocatalysts. *J Phys Chem C*, 2015; 119: 16905-16912. [DOI]
56. Shi W, Zhang R, Wang JC et al. One-pot hydrothermal preparation of Ni and I co-doped brookite-anatase TiO2 nanoparticles with remarkably enhanced photoreduction activity of CO2 to CH4. *J Catal*, 2024; 429: 115235. [DOI]
57. Xie F, Huang C, Dong G et al. One-step hydrothermal synthesis of Zr-doped BT nanorods for highly efficient perovskite solar cells. *Mater Res Bull*, 2024; 173: 112677. [DOI]
58. Katsumata K, Ohno Y, Tomita K et al. Synthesis of amphiphilic brookite nanoparticles with high photocatalytic performance for wide range of application. *Acs Appl Mater Inter*, 2012, 4: 4846-4852. [DOI]
59. Zheng Y, Shi E, Cui S. Hydrothermal preparation of nanosized brookite powders. *J Am Ceram Soc*, 2000; 83: 2634-2636. [DOI]
60. Xu J, Wu S, Jin J et al. Preparation of BT nanoparticles with small sizes and the improved photovoltaic performance of brookite-based dye-sensitized solar cells. *Nanoscale*, 2016; 8: 18771-18781. [DOI]
61. Tay Q, Liu X, Tang Y et al. Enhanced photocatalytic hydrogen production with synergistic two-phase anatase/BT nanostructures. *J Phys Chem C*, 2013; 117: 14973-14982. [DOI]
62. Li K, Xu J, Shi W et al. Synthesis of size controllable and thermally stable rice-like brookite titania and its application as a scattering layer for nano-sized titania film-based dye-sensitized solar cells. *J Mater Chem A*, 2014; 2: 1886-1896. [DOI]
63. Kominami H, Kohno M, Kera Y. Synthesis of brookite-type titanium oxide nano-crystals in organic media. *J Mater Chem*, 2000; 10: 1151-1156. [DOI]
64. Ohno T, Lee SY, Yang Y. Fabrication of morphology-controlled TiO2 photocatalyst nanoparticles and improvement of photocatalytic activities by modification of Fe compounds. *Rare metals*, 2015; 34: 291-300. [DOI]
65. Ma Y, Kobayashi K, Cao Y et al. Development of visible-light-responsive morphology-controlled BT nanorods by site-selective loading of AuAg bimetallic nanoparticles. *Appl Catal B-Environ*, 2019; 245: 681-690. [DOI]
66. Pan J. Synthesis of nitrogen doped faceted titanium dioxide in pure brookite phase with enhanced visible light photoactivity. *J Colloid Interf Sci*, 2016; 469: 25-30. [DOI]
67. Lin H, Li L, Zhao M et al. Synthesis of high-quality BT single-crystalline nanosheets with specific facets exposed: tuning catalysts from inert to highly reactive. *J Am Chem Soc*, 2012; 134: 8328-8331. [DOI]
68. Zhao B, Chen F, Huang Q et al. BT nanoflowers. *Chem Commun*, 2009; 34: 5115-5117. [DOI]
69. Hu W, Li L, Li G et al. High-quality BT flowers: synthesis, characterization, and dielectric performance. *Cryst Growth Des*, 2009; 9: 3676-3682. [DOI]
70. Bellardita M, Di Paola A, Megna B et al. Absolute crystallinity and photocatalytic activity of BT samples. *Appl Catal B-Environ*, 2017; 201: 150-158. [DOI]
71. Tran HTT, Kosslick H, Ibad MF et al. Photocatalytic performance of highly active brookite in the degradation of hazardous organic compounds compared to anatase and rutile. *Appl Catal B-Environ*, 2017; 200: 647-658. [DOI]
72. Perego C, Wang YH, Durupthy O et al. Nanocrystalline brookite with enhanced stability and photocatalytic activity: influence of lanthanum (III) doping. *Acs Appl Mater Inter*, 2012; 4: 752-760. [DOI]
73. Aslan Çakır M, Yetim T, Yetim AF et al. Superamphiphobic TiO2 film by sol–gel dip coating method on commercial pure titanium. *J Mater Eng Perform*, 2024; 33: 1472-1484. [DOI]
74. Fattakhova-Rohlfing D, Zaleska A, Bein T. Three-dimensional titanium dioxide nanomaterials. *Chem Rev*, 2014; 114: 9487-9558. [DOI]
75. Dambournet D, Belharouak I, Ma J et al. Toward high surface area TiO2 brookite with morphology control. *J Mater Chem*, 2011; 21: 3085-3090. [DOI]
76. Du P, Niu P, Yang Y et al. Constructing anatase-BT phase junction by thermal topotactic transition to promote charge separation for superior photocatalytic H2 generation. *J Phys Chem Lett*, 2022; 13: 4244-4250. [DOI]

77. Pottier A, Chanéac C, Tronc E et al. Synthesis of BT nanoparticles by thermolysis of TiCl4 in strongly acidic aqueous media. *J Mater Chem*, 2001; 11: 1116-1121. [DOI]
78. Buonsanti R, Grillo V, Carlino E et al. Architectural Control of Seeded-Grown Magnetic- Semicondutor Iron Oxide- TiO2 Nanorod Heterostructures: The Role of Seeds in Topology Selection. *J Am Chem Soc*, 2010; 132: 2437-2464. [DOI]
79. Zhang Z, Wu Q, Johnson G et al. Generalized synthetic strategy for transition-metal-doped brookite-phase TiO2 nanorods. *J Am Chem Soc*, 2019; 141: 16548-16552. [DOI]
80. Wahi RK, Liu Y, Falkner JC et al. Solvothermal synthesis and characterization of anatase TiO2 nanocrystals with ultrahigh surface area. *J Colloid Interf Sci*, 2006; 302: 530-536. [DOI]
81. Xue B, Sun T, Mao F. Facile synthesis of mesoporous core-shell TiO2 nanostructures from TiCl3. *Mater Res Bull*, 2011; 46: 1524-1529. [DOI]
82. Nematov D, Burhonzoda A, Khusenov M et al. The quantum-chemistry calculations of electronic structure of boron nitride nanocrystals with density Functional theory realization. *Egypt J Chem*, 2019; 62: 21-27. [DOI]
83. Yan XM, Kang J, Gao L et al. Solvothermal synthesis of carbon coated N-doped TiO2 nanostructures with enhanced visible light catalytic activity. *Appl Surf Sci*, 2013; 265: 778-783. [DOI]
84. Ohno T, Higo T, Murakami N et al. Photocatalytic reduction of CO2 over exposed-crystal-face-controlled TiO2 nanorod having a brookite phase with co-catalyst loading. *Appl Catal B-Environ*, 2014; 152: 309-316. [DOI]
85. Jin J, Luo J, Zan L et al. One-Pot Synthesis of Cu-Nanocluster-Decorated BT Quasi-Nanocubes for Enhanced Activity and Selectivity of CO2 Photoreduction to CH4. *ChemPhysChem*, 2017; 18: 3230-3239. [DOI]
86. Xin X, Xu T, Wang L et al. Ti3+-self doped BT single-crystalline nanosheets with high solar absorption and excellent photocatalytic CO2 reduction. *Sci Rep*, 2016; 6: 23684. [DOI]
87. Zhao H, Liu L, Andino JM et al. Bicrystalline TiO2 with controllable anatase–brookite phase content for enhanced CO2 photoreduction to fuels. *J Mater Chem A*, 2013; 1: 8209-8216. [DOI]
88. Li K, Peng B, Jin J et al. Carbon nitride nanodots decorated BT quasi nanocubes for enhanced activity and selectivity of visible-light-driven CO2 reduction. *Appl Catal B-Environ*, 2017; 203: 910-916. [DOI]
89. Chen Z, Zhu X, Xiong J et al. A p-n junction by coupling amine-enriched brookite-TiO2 nanorods with CuxS nanoparticles for improved photocatalytic CO2 reduction. *Materials*, 2023; 16: 960. [DOI]
90. Chen Z, Tong X, Cheng G. A comparative study on metal species implanted amine–brookite–TiO2 nanorods for enhanced photocatalytic CO2 reduction. *Carbon Lett*, 2023; 33: 2041-2051. [DOI]
91. Xiong J, Zhang M, Lu M et al. Achieving simultaneous Cu particles anchoring in meso-porous TiO2 nanofabrication for enhancing photo-catalytic CO2 reduction through rapid charge separation. *Chin Chem Lett*, 2022; 33: 1313-1316. [DOI]
92. Ren X, Gao P, Kong X et al. NiO/Ni/TiO2 nanocables with Schottky/pn heterojunctions and the improved photocatalytic performance in water splitting under visible light. *J Colloid Interf Sci*, 2018; 530: 1-8. [DOI]
93. Jin J, Luo J, Zan L et al. One-Pot Synthesis of Cu-Nanocluster-Decorated BT Quasi-Nanocubes for Enhanced Activity and Selectivity of CO2 Photoreduction to CH4. *ChemPhysChem*, 2017; 18: 3230-3239. [DOI]
94. Xiao J, Chen S, Jin J et al. BT Nanoparticles Decorated with Ag/MnOx Dual Cocatalysts for Remarkably Boosted Photocatalytic Performance of the CO2 Reduction Reaction. *Langmuir*, 2021; 37: 12487-12500. [DOI]
95. Xu J, Li K, Wu S et al. Preparation of brookite titania quasi nanocubes and their application in dye-sensitized solar cells. *J Mater Chem A*, 2015; 3: 7453-7462. [DOI]
96. Xu M, Zada A, Yan R et al. Ti2O3/TiO2 heterophase junctions with enhanced charge separation and spatially separated active sites for photocatalytic CO2 reduction. *Phys Chem Chem Phys*, 2020; 22: 4526-4532. [DOI]
97. Barik SK, Chiu TH, Liu YC et al. Mono-and hexa-palladium doped silver nanoclusters stabilized by dithiolates. *Nanoscale*, 2019; 11: 14581-14586. [DOI]
98. Zhang X, Hu K, Zhang X et al. Surface co-modification with highly-dispersed Mn & Cu oxides of g-C3N4 nanosheets for efficiently photocatalytic reduction of CO2 to CO and CH4. *Appl Surf Sci*, 2019; 492: 125-134. [DOI]
99. Cheng Y, Huang T, Sun Y et al. Catalytic oxidation removal of ammonium from groundwater by manganese oxides filter: Performance and mechanisms. *Chem Eng J*, 2017; 322: 82-89. [DOI]
100. Li Y, Lin L, Mu R et al. Activation of CO over ultrathin manganese oxide layers grown on Au (111). *Acs Catal*, 2021; 11: 849-857. [DOI]
101. Lin LY, Nie Y, Kavadiya S et al. N-doped reduced graphene oxide promoted nano TiO2 as a bifunctional adsorbent/photocatalyst for CO2 photoreduction: Effect of N species. *Chem Eng J*, 2017; 316: 449-460. [DOI]
102. Sorcar S, Hwang Y, Grimes CA et al. Highly enhanced and stable activity of defect-induced titania nanoparticles for solar light-driven CO2 reduction into CH4. *Mater Today*, 2017; 20: 507-515. [DOI]
103. Jin J, Chen S, Wang J et al. One-pot hydrothermal preparation of PbO-decorated brookite/anatase TiO2 composites with remarkably enhanced CO2 photoreduction activity. *Appl Catal B-Environ*, 2020; 263: 118353. [DOI]

104. Liu L, Zhao H, Andino JM et al. Photocatalytic CO2 Reduction with H2O on TiO2 Nanocrystals: Comparison of Anatase, Rutile, and Brookite Polymorphs and Exploration of Surface Chemistry. *ACS Catal*, 2012; 2: 1817-1828. [DOI]
105. Zhao H, Liu L, Andino JM et al. Bicrystalline TiO2 with controllable anatase–brookite phase content for enhanced CO2 photoreduction to fuels. *J Mater Chem A*, 2013; 1: 8209-8216. [DOI]
106. Liao Y, Que W, Jia Q et al. Controllable synthesis of brookite/anatase/rutile TiO2 nanocomposites and single-crystalline rutile nanorods array. *J Mater Chem*, 2012; 22: 7937-7944. [DOI]
107. Chen Z, Xiong J, Cheng G. Recent advances in brookite phase TiO2-based photocatalysts toward CO2 reduction. *Fuel*, 2024; 357: 129806. [DOI]
108. Low J, Yu J, Jaroniec M et al. Heterojunction photocatalysts. *Adv Mater*, 2017; 29: 1601694. [DOI]
109. Wang H, Zhang L, Chen Z. Semiconductor heterojunction photocatalysts: design, construction, and photocatalytic performances. *Chem Soc Rev*, 2014; 43: 5234-5244. [DOI]
110. Yang H. A short review on heterojunction photocatalysts: Carrier transfer behavior and photocatalytic mechanisms. *Mater Res Bull*, 2021; 142: 111406. [DOI]
111. Zhang L, Zhang J, Yu H et al. Emerging S-scheme photocatalyst. *Adv Mater*, 2022; 34: 2107668. [DOI]
112. Jin J, Chen S, Wang J et al. SrCO3-modified brookite/anatase TiO2 heterophase junctions with enhanced activity and selectivity of CO2 photoreduction to CH4. *Appl Surf Sci*, 2019; 476: 937-947. [DOI]
113. Tay Q, Wang X, Zhao X et al. Enhanced visible light hydrogen production via a multiple heterojunction structure with defect-engineered g-C3N4 and two-phase anatase/BT. *J Catal*, 2016; 342: 55-62. [DOI]
114. Li Y, Wen M, Wang Y et al. Plasmonic Hot Electrons from Oxygen Vacancies for Infrared Light-Driven Catalytic CO2 Reduction on Bi2O3−x. *Angew Chem*, 2021; 133: 923-929. [DOI]
115. Li YH, Li JY, Xu YJ. Bimetallic nanoparticles as cocatalysts for versatile photoredox catalysis. *EnergyChem*, 2021; 3: 100047. [DOI]
116. Soltani T, Zhu X, Yamamoto A et al. Effect of transition metal oxide cocatalyst on the photocatalytic activity of Ag loaded CaTiO3 for CO2 reduction with water and water splitting. *Appl Catal B-Environ*, 2021; 286: 119899. [DOI]
117. Zhu S, Liao W, Zhang M et al. Design of spatially separated Au and CoO dual cocatalysts on hollow TiO2 for enhanced photocatalytic activity towards the reduction of CO2 to CH4. *Chem Eng J*, 2019; 361: 461-469. [DOI]
118. Qiu B, Du M, Ma Y et al. Integration of redox cocatalysts for artificial photosynthesis. *Energ Environ Sci*, 2021; 14: 5260-5288. [DOI]
119. Wang J, Lin S, Tian N et al. Nanostructured metal sulfides: classification, modification strategy, and solar-driven CO2 reduction application. *Adv Funct Mater*, 2021; 31: 2008008. [DOI]
120. Li K, Peng B, Peng T. Recent Advances in Heterogeneous Photocatalytic CO2 Conversion to Solar Fuels. *ACS Catal*, 2016; 6: 7485-7527. [DOI]
121. Li X, Jiang H, Ma C et al. Local surface plasma resonance effect enhanced Z-scheme ZnO/Au/g-C3N4 film photocatalyst for reduction of CO2 to CO. *Appl Catal B-Environ*, 2021; 283; 119638. [DOI]
122. Song H, Meng X, Dao TD et al. Light-enhanced carbon dioxide activation and conversion by effective plasmonic coupling effect of Pt and Au nanoparticles. *Acs Appl Mater Inter*, 2018; 10: 408-416. [DOI]
123. Li R, Zhang F, Wang D. Spatial separation of photogenerated electrons and holes among {010} and {110} crystal facets of BiVO4. *Nat Commun*, 2013; 4: 1432. [DOI]
124. Raziq F, Sun L, Wang Y. Synthesis of large surface-area g-C3N4 comodified with MnOx and Au-TiO2 as efficient visible-light photocatalysts for fuel production. *Adv Energy Mater*, 2018; 8: 1701580. [DOI]
125. Meng A, Zhang L, Cheng B et al. TiO2-MnOx-Pt hybrid multiheterojunction film photocatalyst with enhanced photocatalytic CO2-reduction activity. *Acs Appl Mater Inter*, 2018; 11: 5581-5589. [DOI]
126. Zhang XX, Hu K, Zhang XL et al. Photoactivities for CO2 Conversion of g-C3N4 Are Enhanced After Co-Modifying MnOx and CuOx Attributed to Their Roles of Modulating Charges and Providing Catalytic Functions. *Appl Surf Sci*, 2019; 492: 125-134. [DOI]
127. Zhou X, Fang Y, Cai X, Zhang S et al. In Situ Photodeposited Construction of Pt–CdS/g-C3N4–MnOx Composite Photocatalyst for Efficient Visible-Light-Driven Overall Water Splitting. *Acs Appl Mater Inter*, 2020; 12: 20579-20588. [DOI]
128. Molaei M, Fattah-alhosseini A, Nouri M et al. Assessing the wear properties of plasma electrolytic oxidation TiO2 coatings incorporated ZrO2 nanoparticles on Cp-Ti in simulated body fluid. *Appl Surf Sci Adv*, 2024; 19: 100563. [DOI]
129. Meng A, Zhang L, Cheng B et al. Dual cocatalysts in TiO2 photocatalysis. *Adv Mater*, 2019; 31: 1807660. [DOI]
130. Han B, Wei W, Chang L, et al. Efficient visible light photocatalytic CO2 reforming of CH4. Acs Catalysis, 2016; 6(2): 494-497. [DOI]
131. Zhu X, Yamamoto A, Imai S et al. Facet-selective deposition of a silver-manganese dual cocatalyst on potassium hexatitanate photocatalyst for highly selective reduction of carbon dioxide by water. *Appl Catal B-Environ*, 2020; 274: 119085. [DOI]

132. Qiu P, Lu M, Cheng G et al. Co-implantation of oxygen vacancy and well-dispersed Cu cocatalyst into TiO2 nanoparticles for promoting solar-to-hydrogen evolution. *Int J Hydrogen Energ*, 2023; 48: 933-942. [DOI]
133. Yang G, Xiong J, Lu M. Co-embedding oxygen vacancy and copper particles into titanium-based oxides (TiO2, BaTiO3, and SrTiO3) nanoassembly for enhanced CO2 photoreduction through surface/interface synergy. *J Colloid Interf Sci*, 2022; 624: 348-361. [DOI]
134. Gerischer H, Heller A. The role of oxygen in photooxidation of organic molecules on semiconductor particles. *J Phys Chem*, 1991; 95: 5261-5267. [DOI]
135. Wang CM, Heller A, Gerischer H. Palladium catalysis of O2 reduction by electrons accumulated on TiO2 particles during photoassisted oxidation of organic compounds. *J Am Chem Soc*, 1992; 114: 5230-5234. [DOI]
136. Moser J, Punchihewa S, Infelta PP et al. Surface complexation of colloidal semiconductors strongly enhances interfacial electron-transfer rates. *Langmuir*, 1991; 7: 3012-3018. [DOI]
137. Liu L, Jiang Y, Zhao H et al. Engineering coexposed {001} and {101} facets in oxygen-deficient TiO2 nanocrystals for enhanced CO2 photoreduction under visible light. *Acs Catal*, 2016; 6: 1097-1108. [DOI]
138. Li P, Zhou Y, Zhao Z et al. Hexahedron prism-anchored octahedronal CeO2: Crystal facet-based homojunction promoting efficient solar fuel synthesis. *J Am Chem Soc*, 2015; 137: 9547-9550. [DOI]
139. Zhang L, Wang W, Sun S et al. Selective transport of electron and hole among {0 0 1} and {1 1 0} facets of BiOCl for pure water splitting. *Appl Catal B-Environ*, 2015; 162: 470-474. [DOI]
140. Gong XQ, Selloni A. First-principles study of the structures and energetics of stoichiometric BT surfaces. *Phys Rev B*, 2007; 76(23): 235307. [DOI]
141. Zhao M, Xu H, Chen H et al. Photocatalytic reactivity of {121} and {211} facets of BT crystals. *J Mater Chem A*, 2015; 3: 2331-2337. [DOI]
142. Sajan CP, Wageh S, Al-Ghamdi AA et al. TiO2 nanosheets with exposed {001} facets for photocatalytic applications. *Nano Res*, 2016; 9: 3-27. [DOI]
143. Pan J, Wu X, Wang L et al. Synthesis of anatase TiO2 rods with dominant reactive {010} facets for the photoreduction of CO2 to CH4 and use in dye-sensitized solar cells. *Chem Commun*, 2011; 47: 8361-8363. [DOI]
144. Xu H, Ouyang S, Li P et al. High-active anatase TiO2 nanosheets exposed with 95% {100} facets toward efficient H2 evolution and CO2 photoreduction. *Acs Appl Mater Inter*, 2013: 5: 1348-1354. [DOI]
145. Pan J, Liu G, Lu GQ et al. On the true photoreactivity order of {001}, {010}, and {101} facets of anatase TiO2 crystals. *Angew Chem Int Edit*, 2011; 50(9): 2133-2137. [DOI]
146. Liu G, Sun C, Yang HG et al. Nanosized anatase TiO2 single crystals for enhanced photocatalytic activity. *Chem Commun*, 2010; 46: 755-757. [DOI]
147. Qi Y, Zhang F. Overall water splitting over conjugated polymer photocatalysts with crystal facets modulated. *Sci China Chem*, 2020; 63: 1582-1583. [DOI]
148. Dudziak S, Kowalkińska M, Zielińska-Jurek A. Crystal Facet Engineering of TiO2 from Theory to Application. In Updates on Titanium Dioxide. IntechOpen, 2023. [DOI]
149. Nematov D. Titanium Dioxide and Photocatalysis: a Detailed Overview of the Synthesis, Applications, Challenges, Advances and Prospects for Sustainable Development. *J Mod Green Energy*, 2024; 3: 6. [DOI]
150. Huerta-Zerón HD, Rockstroh N, Lang M et al. Photocatalytic CO2 reduction with a TiO2-supported copper photosensitizer and an iron-based CO2 reduction catalyst. *Catal Sci Technol*, 2023; 13: 3940-3945. [DOI]
151. Zhou G, Jiang L, Dong Y et al. Engineering the exposed facets and open-coordinated sites of BT to boost the loaded Ru nanoparticle efficiency in benzene selective hydrogenation. *Appl Surf Sci*, 2019; 486: 187-197. [DOI]
152. ZHANG J, Song YAN, Lu FU et al. Photocatalytic degradation of rhodamine B on anatase, rutile, and brookite TiO2. *Chin J Catal*, 2011; 32: 983-991. [DOI]
153. Tran T, Kosslick H, Ibad F, et al. Photocatalytic performance of highly active brookite in the degradation of hazardous organic compounds compared to anatase and rutile. *Appl Catal B-Environ*, 2017; 200: 647-658. [DOI]
154. Liu Y, Wang Z, Wang W, et al. Engineering highly active TiO2 photocatalysts via the surface-phase junction strategy employing a titanate nanotube precursor. *J Catal*, 2014; 310: 16-23. [DOI]
155. Nguyen TT, Edalati K. Brookite TiO2 as an active photocatalyst for photoconversion of plastic wastes to acetic acid and simultaneous hydrogen production: Comparison with anatase and rutile. *Chemosphere*, 2024; 355: 141785. [DOI]
156. Han B, Wei W, Chang L et al. Efficient Visible Light Photocatalytic CO2 Reforming of CH4. *ACS Catal*, 2016; 6: 494-497. [DOI]
157. Choi M, Yong K. A facile strategy to fabricate high-quality single crystalline BT nanoarrays and their photoelectrochemical properties. *Nanoscale*, 2014; 6: 13900-13909. [DOI]
158. Žerjav G, Žižek K, Zavašnik J et al. Brookite vs. rutile vs. anatase: Whats behind their various photocatalytic activities? *J Environ Chem Eng*, 2022; 10: 107722. [DOI]
159. Vequizo JJM, Matsunaga H, Ishiku T et al. Trapping-induced enhancement of photocatalytic activity on brookite TiO2 powders: comparison with anatase and rutile TiO2 powders. *Acs Catal*, 2017; 7: 2644-2651. [DOI]

 doi:10.20944/preprints202501.1197.v1

160. Akrami S, Watanabe M, Ling TH et al. High-pressure TiO2-II polymorph as an active photocatalyst for CO2 to CO conversion. *Appl Catal B-Environ*, 2021; 298: 120566. [DOI]
161. Janus M, Morawski AW. New method of improving photocatalytic activity of commercial Degussa P25 for azo dyes decomposition. *Appl Catal B-Environ*, 2007; 75: 118-123. [DOI]
162. Chen S, Qian TT, Zhu R et al. Integrating modeling and experimental method for narrowing the optimum phase composition in P25 photocatalyst for typical aromatic pollutants degradation. *Chem Eng J*, 2021; 417: 128061. [DOI]
163. Xiong Z, Lei Z, Li Y et al. A review on modification of facet-engineered TiO2 for photocatalytic CO2 reduction. *J Photoch Photobio C*, 2018; 36: 24-47. [DOI]
164. Chen X, Liu L, Yu PY et al. Increasing solar absorption for photocatalysis with black hydrogenated titanium dioxide nanocrystals. *Science*, 2011; 331: 746-750. [DOI]
165. Niu M, Cheng D, Cao D. Fluorite TiO2 (111) surface phase for enhanced visible-light solar energy conversion. *J Phys Chem C*, 2014; 118: 20107-20111. [DOI]
166. Razavi-Khosroshahi H, Edalati K, Hirayama M et al. Visible-light-driven photocatalytic hydrogen generation on nanosized TiO2-II stabilized by high-pressure torsion. *Acs Catal*, 2016; 6: 5103-5107. [DOI]
167. Wang Q, Watanabe M, Edalati K. Visible-light photocurrent in nanostructured high-pressure TiO2-II (columbite) phase. *J Phys Chem C*, 2020; 124: 13930-13935. [DOI]
168. Peiris S, de Silva HB, Ranasinghe KN et al. Recent development and future prospects of TiO2 photocatalysis. *J Chin Chem Soc*, 2021; 68: 738-769. [DOI]
169. Sohn Y, Huang W, Taghipour F. Recent progress and perspectives in the photocatalytic CO2 reduction of Ti-oxide-based nanomaterials. *Appl Surf Sci*, 2017; 396: 1696-1711. [DOI]
170. Som I, Roy M. Recent development on titania-based nanomaterial for photocatalytic CO2 reduction: A review. *J Alloy Compd*, 2022; 918: 165533. [DOI]
171. Chakroborty S, Nath N, Soren S et al. Plasmonic-based TiO2 and TiO2 nanoparticles for photocatalytic CO2 to methanol conversion in energy applications: current status and future prospects. *Top Catal*, 2024; 67: 232-245. [DOI]
172. Zhang R, Jiang J, Wu W. Wearable chemical sensors based on 2D materials for healthcare applications. *Nanoscale*, 2023; 15: 3079-3105. [DOI]
173. Xi Q, Papaefthimiou V, Le Breton N et al. Influence of Nitridation Conditions on the Doping Sites and Photocatalytic Visible Light Activity of Nb, N-Codoped TiO2. *Chem Mater*, 2024; 36: 3705-3716. [DOI]
174. Fiorenza R, Bellardita M, Balsamo SA et al. A solar photothermocatalytic approach for the CO2 conversion: Investigation of different synergisms on CoO-CuO/BT-CeO2 catalysts. *Chem Eng J*, 2022; 428: 131249. [DOI]
175. Eddy DR, Permana MD, Sakti LK et al. Heterophase polymorph of TiO2 (Anatase, Rutile, Brookite, TiO2 (B)) for efficient photocatalyst: fabrication and activity. *Nanomaterials*, 2023; 13: 704. [DOI]
176. Cao S, Chan TS, Lu YR et al. Photocatalytic pure water splitting with high efficiency and value by Pt/porous BT nanoflutes. *Nano Energy*, 2020; 67: 104287. [DOI]
177. Li J, Wu C, Li J et al. 1D/2D TiO2/ZnIn2S4 S-scheme heterojunction photocatalyst for efficient hydrogen evolution. *Chin J Catal*, 2022; 43: 339-349. [DOI]
178. Meng A, Cheng B, Tan H et al. TiO2/polydopamine S-scheme heterojunction photocatalyst with enhanced CO2-reduction selectivity. *Appl Catal B-Environ*, 2021; 289: 120039. [DOI]
179. Kaseem M, Fattah-alhosseini A. Enhanced the Electrochemical Stability of Al-Zn-Mg Alloy Through the Dual Incorporation of ZrO2 and V2O5 into the Alumina Layer. *Innov Discov*, 2024; 1: 2. [DOI]
180. Li R, Jia Y, Bu N et al. Photocatalytic degradation of methyl blue using Fe2O3/TiO2 composite ceramics. *J Alloy Compd*, 2015; 643: 88-93. [DOI]
181. Xie M, Meng Q, Luan P et al. Synthesis of mesoporous TiO2-coupled Fe2O3 as efficient visible nano-photocatalysts for degrading colorless pollutants. *RSC Adv*, 2014; 4: 52053-52059. [DOI]
182. Jo WK, Selvam NCS. Synthesis of GO supported Fe2O3–TiO2 nanocomposites for enhanced visible-light photocatalytic applications. *Dalton T*, 2015; 44: 16024-16035. [DOI]
183. Yang J, Wang J, Wang G et al. In situ irradiated XPS investigation on S-scheme TiO2/Bi2S3 photocatalyst with high interfacial charge separation for highly efficient photothermal catalytic CO2 reduction. *J Mater Sci Technol*, 2024; 189: 86-95. [DOI]
184. Zhang B, Sun B, Liu F et al. TiO2-based S-scheme photocatalysts for solar energy conversion and environmental remediation. *Sci China Mater*, 2024; 67: 424-443. [DOI]
185. Wang Q, Zhang L, Guo Y et al. Multifunctional 2D porous g-C3N4 nanosheets hybridized with 3D hierarchical TiO2 microflowers for selective dye adsorption, antibiotic degradation and CO2 reduction. *Chem Eng J*, 2020; 396: 125347. [DOI]
186. Shen M, Wang M, Wang Q et al. A Ti-OH bond breaking route for creating oxygen vacancy in titania towards efficient CO2 photoreduction. *Chem Eng J*, 2021; 425: 131513. [DOI]
187. Wang Y, Jiang J, Yao N et al. Enhanced photocatalytic CO2 conversion over 0D/2D AgVO3/TiO2 heterojunctions assisted by Z-scheme charge separation. *Sci China Mater*, 2024; 67: 1820-1829. [DOI]
188. Wang Q, Yang X, Jing Z et al. Recent advances in one-dimensional alkali-metal hexatitanate photocatalysts for environmental remediation and solar fuel production. *J Mater Sci Technol*, 2024; 202: 201-239. [DOI]

 doi:10.20944/preprints202501.1197.v1

189. Zhang L, Zhao Q, Shen L et al. Enhancing the photocatalytic activity of defective titania for carbon dioxide photoreduction via surface functionalization. *Catal Sci Technol*, 2022; 12: 509-518. [DOI]
190. Huerta-Zerón HD, Rockstroh N, Lang M et al. Photocatalytic CO2 reduction with a TiO2-supported copper photosensitizer and an iron-based CO2 reduction catalyst. *Catal Sci Technol*, 2023; 13: 3940-3945. [DOI]
191. Gu H, Liang F, Wang X et al. N-doped rutile TiO2 nanorod@ gC3N4 core/shell S-scheme heterojunctions for boosting CO2 photoreduction activity. *Catal Sci Technol*, 2023; 13: 898-909. [DOI]
192. Eddy R, Permana D, Sakti K. Heterophase polymorph of TiO2 (anatase, rutile, brookite, TiO2 (B)) for efficient photocatalyst: fabrication and activity. *Nanomaterials*, 2023; 13: 704. [DOI]